Deliverable 1.6

Biologically realistic Lagrangian dispersal and connectivity

Project acronym:	ATLAS
Grant Agreement:	678760
Deliverable number:	D1.6
Deliverable title:	Biologically realistic Lagrangian dispersal and connectivity
Work Package:	WP1
Date of completion:	28 December 2018
Author:	Alan Fox, University of Edinburgh Stefan Gary, SAMS Arne Biastoch, GEOMAR Stuart Cunningham, SAMS J. Murray Roberts, University of Edinburgh

This project has received funding from the European Union's Horizon 2020 research and innovation programme under grant agreement No 678760 (ATLAS). This output reflects only the author's view and the European Union cannot be held responsible for any use that may be made of the information contained therein.

Contents

List of Tables

List of Figures

Summary

- Larval behaviours are predicted to impact their long-term spreading, with wider spreading being everywhere associated with more time spent higher in the water column.
- The strength of this enhanced dispersal varies regionally (from strong to very strong).
- Dispersal pathways are predicted to be affected by larval behaviour in ways which could influence the distribution of species.
- For deep-sea populations, the uncertainty in modelled dispersal and connectivity associated with vertical larval positioning in the water column is potentially an order of magnitude larger than that associated with pelagic larval duration or model hydrodynamics.
- The knowledge gaps in larval behaviour which contribute most to the uncertainty concern settling – the age at which larvae start to sink, and the sinking rate.
- In the absence of detailed knowledge of larval development, time-series observations of larval position in the water column could be used to constrain models, hugely reducing uncertainty in predictions.
- Under the most dispersive behaviour modelled, populations throughout the North Atlantic would be connected. Seamount populations may be crucial stepping stones in this wider connectivity.
- In the more dispersive scenarios two large-scale closed connectivity loops were identified, one anticlockwise around the North Atlantic basin with west-east return via the Azores, the second smaller loop following the sub-polar gyre.
- Even for the least dispersive behaviour modelled, populations along the continental slope may be connected anticlockwise around the North Atlantic, de-

pending on the detailed habitat distribution.

- These conclusions are based on a large, systematic Lagrangian modelling experiment, tracking about 10 million virtual particles over 50 years in contrasting dynamical regimes around the North Atlantic Ocean.

1 Introduction

Many ocean bottom dwelling species release their larvae into the water column so that the larvae can both be recruited into the local population and spread further afield to support remote populations and colonize new sites. A better understanding of larval pathways and downstream colonization is an important factor determining population connectivity, informing studies of natural and man-made networks, feeding into the design of Marine Protected Area networks and ultimately impacting how the marine environment is used. During their transit, larvae exhibit a range of different behaviours for maximizing their immediate survival (finding food and avoiding predation) and their long-term survival (finding a suitable spot to settle). Key strategies are pelagic duration and control of the vertical position in the water column.

Connectivity of marine ecosystems is fundamental to survival, growth, spread, recovery from damage and adaptation to changing conditions, on ecological and evolutionary timescales (James et al. 2002; Cowen and Sponaugle 2009; Burgess et al. 2014). Empirical evidence shows the benefits of connectivity information to conservation management (Planes et al. 2009; Olds et al. 2012). Knowledge of the characteristics of marine connectivity is rapidly expanding, with recent studies using seascape genetics approaches combining particle tracking in high resolution ocean models with state-of-the art genetic techniques (Foster et al. 2012; Teske et al. 2016; Truelove et al. 2017). Many populations in the deep sea are spatially fragmented and vulnerable to damage from increasing exploitation of the deep sea; understanding the connectivity between the subpopulations is critical for spatial management (see

Cabral et al. 2016, for a review). But knowledge of deep sea connectivity remains limited – from both the physical and biological perspective. Direct evidence of deep sea population connectivity, through tagging and tracking, remains almost unknown, but indirect estimates of connectivity can be constructed by using genetic methods, elemental fingerprinting or particle modelling.

A common indirect method of estimating connectivity is through tracking of virtual adults, juveniles or, more usually, larvae, within a hydrodynamic model – so called 'Lagrangian', individual-based models (IBMs) or particle tracking modelling. To date, in the deep sea, this approach is limited to relatively few studies (e.g. Lavelle et al. 2010; McGillicuddy et al. 2010; Yearsley and Sigwart 2011; Young et al. 2012; Fox et al. 2016; Breusing et al. 2016). Such modelled connectivity and dispersal estimates are affected by life history traits – timing of spawning, larval behaviour, and effective pelagic larval duration (PLD). Knowledge of these biological parameters, and estimates of their relative importance to dispersal and connectivity in the deep sea is sparse. Bradbury et al. (2008) review estimates of marine dispersal, for fish species estimates are primarily based on otolith microstructure and show a correlation between habitat depth and PLD – fishes living at deeper depths have generally longer PLD. For non-fish species, Bradbury et al. (2008) estimated PLD from biogeography and population separation distances.

Hilário et al. (2015) provide a thorough, updated review of the challenges of estimating dispersal distances in the deep sea. They found estimates of PLD in the literature for fewer than 100 species living below 200m, over 80% of these estimates are for species on sedimentary slopes, predominantly echinoderms. PLDs from a few days to over a year were found. Direct observations of larval position in the water column has also been used to infer PLD and spawning times and to ground-truth larval dispersal models (Mullineaux et al. 2005; Arellano et al. 2014), predominantly for species of mollusc (with larger, more substantial larvae) living around vents and seeps.

Dispersal depth is also thought to be a critical parameter for deep-sea connectiv-

ity, since current speeds, directions and turbulence can vary significantly with depth. For example, Lagrangian modelling demonstrates that larvae of the deep-sea mussel "Bathymodiolus" childressi drifting in the upper water layers of the Gulf of Mexico can potentially seed most known seep metapopulations on the Atlantic continental margin, whereas larvae drifting demersally cannot (McVeigh et al. 2017). In the northeast Atlantic, Fox et al. (2016) showed how *Lophelia pertusa* larvae following vertical swimming behaviour traits predicted from observations in the laboratory (Larsson et al. 2014; Strömberg and Larsson 2017) may disperse much more widely than passive larvae.

The occurrence of seep species of molluscs, crustaceans, and other taxonomic groups across the Atlantic Ocean suggest broad connectivity (e.g. Cordes et al. 2007), while recent examination of deep-sea sponges in the NE Atlantic (Soest and Voogd 2015) finds communities at Mingulay were faunistically closer to the geographically-distant shelf reefs at Skagerrak than to the geographically closer bathyal reefs of the Porcupine–Rockall area. The Atlantic meridional overturning circulation (AMOC) can achieve large-scale larval dispersal across ecological timescales as observed in the cold-water-coral *L. pertusa* (Henry et al. 2014). Dispersal modelling, coupled with pelagic larval duration estimates and population genetics, has also recently (Young et al. 2012; Breusing et al. 2016) been used to predict the existence of further vent ecosystems between neighbouring known sites on the mid-Atlantic ridge.

Hilário et al. (2015) identify the physical component of biophysical connectivity models as one of the gaps in estimating deep sea connectivity. While these models are far from perfect, the errors are better defined than those associated with the larval biology, with widespread verification against, and assimilation of, in-situ and remotely sensed data covering many variables at all depths. These models are described in detail in the physical oceanography and modelling literature, output from many is available online. Of more concern is the risk that ecologists use such models as a 'black box', choosing a model which appears to work but whose inner workings are unknown, potentially resulting in misuse and misunderstanding of the models

capabilities (Ross et al. 2016). The current generation of global- and basin-scale models run at horizontal resolutions of 3–4 km, modelling mesoscale eddies, and, when used for particle tracking, are able to reproduce the coherent structures, patch stretching and straining, attractors and barriers described by Harrison et al. (2012). Of particular concern in the deep-sea is the difficulty in modelling the small-scale turbulence, mixing and cross-slope exchanges associated with the steep topography (upper continental slope, seamounts and ocean ridges) which forms typical adult habitat and which may be fundamental to early-life larval dispersal and later settling.

As outlined above, for deep sea species observational evidence of the characteristics of the larval behaviour strategies are severely lacking, while the little evidence available suggests these strategies to be important for larval dispersal and population connectivity. Particle tracking modelling can perhaps be most useful for predicting which larval behaviour traits have the strongest influence on larval dispersal, and thereby helping to guide future observational work.

Working with the ATLAS Case Study regions in the North Atlantic, we try to answer two questions to help identify whether larval behaviours are impacting their long-term spreading: Is there any evidence that any of these behaviours, either alone or combined, cause greater spreading? And, do any of these behaviours cause larvae to follow particular pathways so they settle in specific locations? To answer these questions we use particle tracking with ARIANE within the VIKING20 model of the North Atlantic.

2 Methods

Particles are simulated with a modified version of the ARIANE software (Döös 1995; Blanke et al. 1999) coupled to the velocity, potential temperature, T, and salinity, S fields in the VIKING20 configuration (Böning et al. 2016) of the NEMO ocean model (Madec 2008). In the VIKING20 hindcast run, forced by the CORE2 data set (Large and Yeager 2009), a 0.05° resolution grid spanning the North Atlantic

was two-way nested (Debreu et al. 2008) within a 0.25° resolution global ocean. VIKING20 output from 1958 to 2009, at a temporal resolution of average fields over every 5 days, is used here. Modifications have been added to ARIANE by Alan Fox and Stefan Gary to include independent vertical motion of particles (https://github.com/alanfox/ARIANE_Larvae_1.0), simulating the ability of organisms to actively swim or control their buoyancy. This allows individual control of vertical behaviour for each particle.

Our control dataset is 9.2 million, 1 year-long, passive particle tracks launched from the 12 ATLAS Case Study sites, which was completed for ATLAS Deliverable 1.1 (https://doi.org/10.5281/zenodo.570588) . In the control run, all particles are purely advective; their movement is entirely dependent on the VIKING20 velocity field. From the deep-sea literature (e.g. Hilário et al. 2015; Mullineaux et al. 2005; McVeigh et al. 2017; Larsson et al. 2014; Brooke and Young 2005) we have identified 5 key larval behaviours that are varied systematically between simulations. Using high and low representative values of each behaviour, a sweep of the possible combinations of behaviours results in 2^5 (= 32) runs.

As for ATLAS Deliverable 1.1, model experiments here are based on releases from the ATLAS Case Study regions (Figure 1), with particles released over a range of depths representing species and habitats being studied in ATLAS (depth ranges of interest were obtained from the ATLAS Case Study groups and are shown in Table 1). The distribution of Case Study regions enables us to study the effects of larval behaviour in a range of dynamical regimes representative of 300–2000 m depth range in the North Atlantic, including offshore banks and seamounts, east and west Atlantic shelf slope, the mid-Atlantic ridge and shallower sites on the shelf.

The common behaviour traits identified for this study are:

1. 'Age of maturity'. The age at which full swimming ability is attained, or maximum positive buoyancy. Range [0,10 days]. Zero represents buoyant eggs for example, 10 days is the approximate age of full swimming ability observed in *L. pertusa* larvae (Larsson et al. 2014).

2. 'Age of competency'. The age at which larvae start heading downwards, to find somewhere to settle. Range [4 days, 42 days]. This range was chosen to cover larvae which head downward early (e.g. *Oculina varicosa* Brooke and Young 2005) and those which descend later (e.g. *L. pertusa* Larsson et al. 2014). Extrapolation to longer periods is possible from the results.

3. Upward speed. The peak upward swim (or buoyancy driven) speed achieved after the age of maturity. Speed increases linearly from age zero until the age of maturity. This is in addition to any vertical advection by the model flows. Range [$0.2\,\mathrm{m\,s^{-1}}$, $1.0\,\mathrm{m\,s^{-1}}$], to reproduce a range of behaviours from slow ascent (slightly buoyant) mostly to move particles clear of the bed, to significant upward movement towards the upper end of speeds observed in the laboratory (Strömberg and Larsson 2017; McVeigh et al. 2017).

4. Downward speed. As for upward speed except downward. This is the speed of descent after the age of competency. Range [$-0.2\,\mathrm{m\,s^{-1}}$, $-1.0\,\mathrm{m\,s^{-1}}$], to represent the range from slight downward drift to return to the bed to strong downward swimming.

5. Target depth. The depth below the surface at which larvae stop heading upwards. Once this depth is attained particles can still be advected vertically by the model flows. Particles thus advected below the target depth restart upward swimming, so once reached the target depth effectively sets a maximum drifting depth. Range [6 m, 120 m], this range was chosen to investigate the possible effects of near-surface wind-driven Ekman layer flows on particle dispersal.

All particles were tracked in the model for 6 months (185 days). Tracks can then be curtailed at any age to simulate different maximum larval lifespans. At the bed, downward swimming is phased out smoothly in the next-to-bottom gridbox and set to zero in the bottom gridbox, so particles near the bed continue to drift in the near-bed currents. Such near-bed particles can still be advected vertically by the

model flows. Competent, near-bed particles advected back into the model interior will resume downward swimming.

This gives a total of 32 tracking experiments, with each trait varying independently. These were run on the Edinburgh University "Eddie" cluster. The 32 behaviours are listed in Table 2 together with a line colour and style key to subsequent figures. Figure 2 shows these behaviours schematically.

Particle tracks are stored in netcdf format and the post-processing and visualization of the larval simulations has been performed in python using numpy, matplotlib and cf-python packages. This involved four stages:

- Split output particle trajectories into subsets specific to each of the ATLAS Case Study regions and to each season of release (DJF, MAM, JJA, SON, seasonal results are not presented here).

- Quantify the spreading rates of larvae with age and the overall spreading after 6 months from each Case Study over each season or in aggregate. 2D histograms of particle positions from the particle tracks are constructed. The spreading is quantified by the smallest area within the contours enclosing 100%, 95%, 90%, 80% and 50% of the particle positions over time (Breusing et al. 2016).

- Apply a "survival filter" which will use the depth of each particle relative to the bottom of the ocean to determine when along each trajectory the larval particle is in a location that it could settle and survive. Temperature and salinity are recorded along-track and species-appropriate ranges could be added to these survival filters.

- Determine whether any combination of behaviours favours specific pathways by using the histograms constructed in step 3.

To efficiently visualize the salient characteristics of each combination of larval behaviours, we computed two indices based on the growth of the area over which the larvae spread. The first index, area growth, is simply the difference between the

areas of the 95% confidence contours that enclose the larvae after 185 days, A_f, and at the beginning of the simulation, A_i:

$$\text{area growth} = A_f - A_i \tag{1}$$

The area growth index, presented here in units of km^2, is an estimate for the spreading range of the larvae with a particular set of behaviours from each Case Study site. Negative values would indicate overall contraction in area, but they do not occur here. The second index, relative curvature, is a measure of the extent to which larvae with a given set of behaviours experience a change in diffusive regime during their 185 day spreading simulation:

$$\text{relative curvature} = \frac{\int_{t=0}^{185}(A(t) - A_i)dt - 0.5(A_f - A_i)\Delta t}{0.5(A_f - A_i)\Delta t} \tag{2}$$

where $A(t)$ is the area enclosing 95% of the larval positions at a given time step, t, and Δt is the 185 day duration of the simulation. Graphically, the relative curvature index is the area between the curve defined by the time series of larval spreading area with respect to a line from A_i to A_f normalized by the area under the line from A_i to A_f. For the highly simplified case of pure diffusion, the spreading area of the larvae would grow linearly in time so the line from A_i to A_f is a useful reference point. The relative curvature index is designed to highlight significant changes in the slope of $A(t)$ which would indicate changes in the effective diffusion experienced by the larvae. Since the relative curvature index is normalized, it is dimensionless. A relative curvature index of 0 indicates that $A(t)$ is exactly the same as the reference line while positive (negative) values suggest stronger (weaker) initial area growth followed by weaker (stronger) growth near the end of the larval paths.

3 Results

3.1 Dispersal pathways

Figures 3 to 14 show the 2D histograms of particle dispersal at age 6 months for two behaviours: types 12 and 21 (Table 2). Type 12 behaviour, solid black line in Figure 2, produces particles which spend the maximum possible amount of time nearest to the surface: rising quickly from age zero, drifting in the surface 6 m until age 42 days, then descending slowly. We will refer to this below as 'near-surface' behaviour. Type 21 behaviour, in contrast, produces demersal behaviour with particles spending the maximum amount of time at the bed: rising slowly for just 4 days before descending rapidly and remaining near the bed. We will refer to this behaviour type as 'demersal' behaviour. These represent the two behaviour extremes modelled, so we expect the resulting distributions to represent the dispersal extremes. This is confirmed from examination of the full set of histograms (not shown).

For all the Case Study regions, following the near-surface strategy results in significantly wider dispersal than the demersal strategy. The difference ranges from slightly wider near-surface spreading extent for the shallower, shelf/shelf break sources in the northeast (CS01:LoVe and CS04:Mingulay), through significantly wider near-surface spreading for most sources on the eastern and northern Atlantic slope and banks, to hugely increased near-surface dispersal for the sources near the western boundary currents (CS11:Flemish Cap and CS12:US Mid-Atlantic canyons). These differences reflect the different flow strengths around the basin, with the eastern North Atlantic having generally weaker and more barotropic flows than in the west. Particles rising towards the surface from CS11 (Flemish Cap) and CS12 (US Mid-Atlantic Canyons) can enter the strong currents and highly turbulent regime of the Gulf Stream and North Atlantic Current, resulting in much wider dispersal.

Behaviour also has significant impact on the particle dispersal pathways from most Case Study sources:

CS01 LoVe. Near-surface behaviour (Figure 3a) produces increased numbers of particles travelling north along the continental slope to the southwest of Svalbard, and into the shallower waters north of CS01. In contrast, demersal behaviour (Figure 3b) increases particle transport southwards along the continental slope.

CS02 West Shetland Slope: Similarly to CS01, a near-surface strategy (Figure 4a) favours transport pathways north and west, while a demersal strategy (Figure 4b) favours pathways eastward along the Iceland-Faroe Ridge to the Reykjanes Ridge south of Iceland.

CS03 Rockall Bank. Near-surface behaviour (Figure 5a) predominantly produces wider spreading than demersal (Figure 5b), but potentially extends spreading (dark blue colours indicating few particles in Figure 5a) onto the shelf around Scotland, into the northern North Sea and across to the coast of Norway.

CS04 Mingulay. Larval behaviour appears relatively unimportant for dispersal pathways (Figures 6a and 6b).

CS05 Porcupine Seabight. Near-surface spreading (Figure 7a) opens up pathways into the Irish Sea and North Sea, to the Scottish west coast, Norwegion coast, southeastern Rockall Bank and the Reykjanes Ridge. Under demersal spreading (Figure 7b) modelled particles are confined closely to the shelf and slope west of Ireland.

CS06 Bay of Biscay. Modelled particle dispersal is quite weak, particularly for demersal behaviour where spreading barely extends beyond the source region (Figure 8b). Near-surface behaviour extends spreading all in directions but particularly northwards in the slope current (Figure 8a).

CS07 Gulf of Cádiz and Alboran Sea (Figures 9a and 9b). Looking separately within and outwith the Mediterranean: within, a near-surface strategy generally increases dispersal but with no obvious favoured pathways; outside, demersal dispersal is weak, a near-surface strategy produces two clear pathways – north-

wards along the coast and southeastwards. More detailed examination of other behaviour strategies (not shown) suggests that the southeast path is associated with drift within the surface 100 m, with the northward path associated with drift at intermediate depths.

CS08 Azores. Near-surface dispersal just increases dispersal distance in all directions (Figures 10a and 10b), with no obvious dispersal pathways reflecting the generally weak mean flows.

CS09 Reykjanes Ridge. Again a near-surface behaviour increases dispersal (Figures 11a and 11b). The major pathway is unchanged though, following the slope westwards. Near-surface dispersal may produce a weak pathway between Iceland and Greenland to the north coast of Iceland.

CS10 Davis Strait. The main pathway is southwards from the source for all behaviours (Figures 12a and 12b), with little change in distance covered.

CS11 Flemish Cap. Particle dispersal is radically different between near-surface and demersal dispersal (Figures 13a and 13b). Demersal dispersal is weak but predominantly southwestwards. Near-surface dispersal is much stronger, the southwest pathway is extended (more than doubled in length), but dispersal also increases to the North and East into the Labrador Sea and across to Reykjanes Ridge.

CS12 US Mid-Atlantic Canyons. Again predicted demersal dispersal is weak and mostly southwards (leaving the southern boundary of our fine resolution model region (Figure 14b)). Near-surface dispersal (Figure 14a) is very strong to the east and north, reaching Bermuda, Atlantic seamounts and almost reaching the Azores (a slightly longer period in the surface layer would predict connections to the Azores).

3.2 Behaviour traits, dispersal rates

For idealised horizontal turbulent dispersal from a point source, with a constant, spatially uniform diffusion coefficient, the area of spread of particles is predicted to grow linearly (with gradient determined by the diffusion coefficient). While the ocean is far from being in such an idealised state (even our modelled ocean) it is interesting to examine the spreading rates of particles from each case study region in our passive, control experiment (Figure 15). These confirm this general relationship of spreading area growing linearly with time. The areas which perhaps conform least to this model are CS12 (US Mid-Atlantic Canyons) where initial spreading rates (for the first 25 days) are low, and CS04 (Mingulay) where spreading accelerates beyond about 25 days. The likely explanation in both cases is particles moving into more dynamically active regimes: getting entrained into the Gulf Stream from CS12, and into the stronger slope current slightly offshore from Mingulay. Note that while spreading areas increase linearly with time, t, spreading radius – more relevant to connectivity studies – increases more slowly with $\sqrt{t}$. This potentially reduces uncertainty in connectivity estimates compared to that in pelagic larval durations (PLDs) on which they may be based.

3.2.1 General influence of behaviour traits on dispersal

Figures 16 to 27 show the changes in dispersal areas against time (dispersal rates) along with the mean depth in the water column of the particles, for each of the 12 Case Study regions and all 32 behaviours. Figures 28 to 29 summarize the dispersal rates figures by plotting the area growth index versus the relative curvature index for each Case Study and for each combination of larval behaviours. The influence of behaviour traits on dispersal areas has some features which are common to dispersal from almost all Case Study regions, we will highlight these first before examining how the individual Case Study regions differ from this base.

Case Studies 3, 8 and 12 (Rockall Bank, Azores and US Mid-Atlantic Canyons) most clearly demonstrate the general influence of the different behaviour traits (all

other Case Study regions contain small variations discussed below, except for Case Study 4, Mingulay, which shows a quite different response). The fastest, and as a result the overall widest, spreading is generally achieved by behaviour type 12, which is also the behaviour with particles closest to the surface (solid black lines in Figures 16 to 27). The details of Type 12 behaviour are: zero age of maturity; late, 42 day, age of competence; fast, 1.0 mm s^{-1}, upward swimming; slow, 0.2 mm s^{-1}, downward swimming; and surface, 6 m target depth. The greatest spreading of Type 12 is also clear in Figure 29 where the black symbols almost always correspond to the greatest area growth in each Case Study. In order of the size of the effect after 6 months, the influence of the 5 behaviour traits can be ranked:

1. Age of competence. Particles that start swimming down early – red/purple lines and symbols – have much reduced dispersal rates over the first 100 days or so than those swim upwards and remain at the surface for longer – black/blue lines and symbols (Figure 29).

2. Downward swimming speed. Shown by pale lines (grey vs. black, pink vs. red, pale blue vs. blue, pale purple vs. purple), rapid descent slows dispersal rates much more quickly than slow descent. This effect often continues even once all particles are near the bed (for example compare the gradients of dark and pale lines of each colour after 150 days in Case Study 03 (Figure 18a)). While faster descents tend to reduce the total spreading area, they add more variability to the change in diffusive regime compared to slower descents (Figure 29).

3. Upward swimming speed. Slow upward swimming is shown by the addition of blue to the line colours, so compare blue (slow upward) with black (fast upward) and purple (slow upward) with red (fast upward). Slower upward swimming speed produces lower dispersal rates in the early life of the particles, the resulting reduced spreading is then generally maintained beyond the age of competence.

These three behaviour traits produce the vast majority of variability in spreading

in most of the case studies. The remaining two behaviour traits produce only minor changes. In particular, in many cases with early age of competence (red/purple lines), the effects of these behaviour traits is so small that the different lines cannot be seen in the figures (e.g. dotted lines lost when coincident with solid lines). The minimal impact of age of maturity and target depth is also evident at a glance in Figures 28 and 29 where symbols with the same colour, but different symbol types, are grouped together.

4. Target drifting depth. A deeper, 120 m, target drifting depth (dotted lines) generally slightly reduces spreading compared to drifting at the surface (6 m), solid lines. Exceptions to this are discussed below.

5. Age of maturity. Later, 10 days, age of maturity (at which maximum vertical swim speed is reached, dashed lines) slightly reduces initial spreading, the only case where this is really significant is if combined with early competence and fast upward swimming (red lines vs. red dashed lines). A small burst of rapid upward motion initially can significantly increase spreading, specially when coupled with subsequent slow descent. Later age of maturity excludes this initial rapid ascent.

For all the runs based on behaviour types with later, 42 day, age of competence (black- and blue-based lines), the other behaviour traits appear to operate almost independently, with the magnitude of the effects of each simply adding up. The situation is less clear with early age of competence as behaviour traits then interact more (for example target depths may never be reached, and later age of maturity makes little difference with slow upward swimming over short times).

Figures 16 to 27 also include the spreading of particles from the passive, control run. In all Case Studies, except Mingulay (CS04), in the first 50 days passive particles spread at speeds at or just slightly faster than those with early-competency near-bed behaviours, significantly more slowly than the rapidly-ascending, late-competency particles. Beyond 50 days, the passive particles do not sink towards the bed, so their spreading continues at a higher rate making comparisons more

difficult in this time range. For Mingulay releases (Figure 19), passive particles produce the widest spreading. It may be that, in the well-mixed shallow shelf waters, behaviour which confines particles to just part of the water-column, either surface or bed, reduces dispersal rates.

The overwhelming general pattern is that particles nearer the surface disperse more quickly, and particles closer to the bed disperse more slowly. This recurring theme can be seen by comparing the spreading rates in the (a) panels with the mean particle depths in the (b) panels in Figures 16 to 27 as well as comparing the blue/black points in Figures 28 to 29 to the other points. Interestingly, there is at best only a weak relationship between the area growth index and the relative curvature index suggesting that simply achieving dramatic changes in exposure to diffusive regime is not the key to wide dispersal. Rather, the approach of "slow and steady wins the race" where the larvae that maximize their time at near the surface tend to spread the farthest without necessarily achieving the greatest change in diffusive regime.

3.2.2 Variations from the general pattern

Particle dispersal from Mingulay appears quite different to the other 11 sites, and is described further below. Within the 11 more 'standard' sites there are examples where specific behaviour traits have more or less influence than average. In particular responses to upward swim speed and target depth seem to vary quite strongly between source regions. Upward swim speed (blue lines vs. black lines) has less influence on dispersal rates in the shallower source regions (Case Studies 1,2 and 5, Figures 16, 17 and 20) and more influence in the deepest regions (Case Study 11, Figure 26). This reflects the shorter time taken to reach the surface from shallower source regions even at slower speeds. Target depth has more influence than average on spreading rates in Case Study regions 5 (slight), 6, 7 and 10 (Figures 20 to 22 and 25). This reflects stronger vertical variation in the near-surface currents and turbulence regimes in these areas.

A couple of further site-to-site differences can be seen. Firstly, at some sites spreading continues quite strongly towards the end of the 6-month period when the largest proportion of particles will be near the bed (most markedly in Case Studies 1, 2 and 9, Figures 16, 17 and 24). These are either shallower areas, or areas with stronger deep flows. Secondly, the mean particle depths at the end of the six month dispersal vary strongly with behaviour at many, but not all, sites (Case Studies 1, 2, 6, 7, 8, 10, 11 and 12, (b) panels in Figures 16 to 27). These mean depths are not simply related to dispersal area and are further evidence of the different dispersal patterns driven by variations in particle behaviour.

3.2.3 Case Study 4, Mingulay

Particle behaviour makes relatively little difference to the area of dispersal, a factor of 2 between weakest and strongest dispersal from Mingulay compares with a factor of over 100 at Flemish Cap. Within this weaker variability, dispersal rates from Mingulay releases (Figure 19) follow a quite different pattern to all other source sites. While at all other sites the strongest driver of differences in overall dispersal extent is age of competency (red lines vs. non-red lines), at Mingulay the strongest driver is descent speed (pale lines vs. dark lines), with rapid descent reducing spreading rates. Strong swimming to the surface for a long period (black and blue, dark, solid and dashed lines) also seems to slow spreading. The most dispersal is found in those behaviours where particles swim weakly, starting from an early age of competency, or those with a target depth of 120 m. The reason seems to be that deeper target and weaker downward swimming lead to a larger range of different depths occupied (rather than particles being closely confined to surface or bed). In the on-shelf, more barotropic environment, this wider vertical distribution appears to be the driver of wider dispersal.

3.3 Connectivity

The dispersal results described above are based on all particles released from each site. No account has been taken of whether the dispersal is 'useful': returning particles to the source region or providing settling particles to other suitable habitats. In Figures 3 to 14, panels (c) and (d) we include only those particles which return to the bed (defined as being within the bottom 2 model layers) at the end of 6 months, and shading of depths below 2200 m serves as a guide (albeit an imperfect one) to the extent of suitable habitat for settling.

The habitats and species being studied in ATLAS generally live on banks, seamounts and continental slope at depths of 200 m to 2000 m. This potentially provides a continuous arc of connected suitable habitat from the Gulf of Cádiz, anticlockwise round to the US Mid-Atlantic Canyons. This arc could remain connected under all the behaviour types explored here, depending largely on the (unknown) details of species distributions.

More interesting are potential connections across the larger gaps across unsuitable habitat, particularly to and from the Azores and the Mid-Atlantic Ridge. Releases from Case Study 8, Azores (Figure 10 (c),(d)), show some connectivity along the Mid-Atlantic ridge, northwards and southwards, for even the least dispersive behaviours (Figure 10d). So again continuous connectivity will depend on details of species and habitat distributions. More dispersive behaviour (Figure 10c) predicts connection from the Azores eastward to seamounts on the Madeira-Tore Rise. This area is also predicted to receive more dispersive particles from the Gulf of Cádiz (Figure 9c), potentially forming a stepping-stone for dispersal in both directions between the Azores and the European continental slope.

Connections from the Azores westward to the North American Atlantic slope look unlikely under all behaviour types, even allowing for stepping-stones. Connections from the North American Atlantic slope to the Azores appear possible under the more dispersive, near-surface behaviours. Releases from the US Mid-Atlantic Canyons (Figure 14d) show particles almost reaching the Azores, and easily reaching

Bermuda, New England Seamounts and Corner Rise Seamounts. Considering the strong eastward surface dispersal, releases from these stepping-stone areas might be expected to reach the Azores. Similarly, while particles released from Flemish Cap are not predicted to directly cross to the Azores, but under more dispersive behaviour types reach potential seamount stepping-stones. Flemish Cap releases are also predicted to reach the Mid-Atlantic Ridge north of the Azores and the southern tip of the Reykjanes Ridge, potentially providing a smaller, stepwise circulation of larvae around the subpolar gyre.

4 Discussion

The dispersal and connectivity results presented here represent the first large-scale, systematic, predictions of how some common life history traits of pelagic larvae of deep-sea species could affect dispersal and connectivity. The life history traits examined controlled the vertical position of larvae in the water column in time. The major conclusion is that in all regions studied except shallow shelf seas, larvae which rise towards the surface disperse more widely than those which remain at depth. We also see potential changes in pathways governed by larval behaviour. The wider dispersal seen in surface-travelling particles is separate, and in addition to, possible wider dispersal resulting from longer larval lifespan.

Comparing these results with known species distributions, the wide distribution and genetic similarities of *L. pertusa* (e.g. Dahl et al. 2012) would support the distribution strategy suggested by laboratory experiments (Larsson et al. 2014; Strömberg and Larsson 2017). Our results support recent results on sponge species composition in the Northeast Atlantic (Soest and Voogd 2015) and suggest long larval PLD rather than dispersal in surface waters, with sponge community composition changing more between sites on and off the shelf than over long distances on-shelf. Our results may also have implications for the conclusions of Breusing et al. (2016), inferring the presence of "Phantom" stepping stones connecting Mid-Atlantic Ridge vent ecosystems.

With data on life history traits and vertical movement of larvae from deep-sea species being scarce and difficult to gather (Hilário et al. 2015; Bradbury et al. 2008), it is useful to consider how this lack of information might affect dispersal and connectivity estimates in comparison with uncertainties in modelled dynamics and larval lifespans. The default approximation when modelling deep-sea larval dispersal remains one of passive larvae (e.g. Breusing et al. 2016), with the behaviour parameters are reduced to a single one, pelagic larval duration (PLD). A doubling of PLD will typically result in a doubling of area of dispersal, and a corresponding, smaller increase in connection radius of a multiple of $\sqrt{2}$. In the shelf seas (Case Study 4, Mingulay example above), we suggest the uncertainty in dispersal area associated with vertical positioning of larvae is of a similar order. However for deeper, off-shelf, populations the uncertainty associated with vertical positioning in the water column is potentially an order of magnitude larger.

Comparison of modelled Lagrangian particle tracks with ground truth data, for example individual Argo float tracks, is difficult - small initial position errors and missing model dynamics are quickly amplified. However, when large numbers of virtual particles are released, Lagrangian models have proved adept at reproducing distributions of, for example, drifting buoys, marine litter, and nutrient concentrations (e.g. Wang et al. 2018; Sebille et al. 2018; Cetina-Heredia et al. 2018; Hardesty et al. 2017; Hart-Davis et al. 2018). The current study uses hydrodynamic fields from a high resolution, 0.05° model (VIKING20), with many millions of particles released over 50 years. Perhaps the major potential source of uncertainty in the model is in the near-bed flows, crucial to modelling the settling phase of larval life. VIKING20 does not model the bottom boundary layer, Breusing et al. (2016) found precise choice of release site in VIKING20 was required to realistically model larvae released from vent sites on the Mid-Atlantic Ridge. The larger release areas used here should mitigate against this uncertainty in initial dispersal, but conclusions about continued spreading once particles have returned to the bed should be treated with caution. We therefore estimate uncertainties due to hydrodynamic

model in the results presented here, obtained from release of many particles, should be lower than the uncertainties associated with either PLD or vertical behaviours.

The large uncertainties in larval behaviour make it difficult use observations of population connectivity – for example from genetics – to infer details, or put bounds on, individual larval behaviour traits. In some extreme examples this may be possible – for example in the western Atlantic where dispersal at depth and near-surface may go in opposite directions. More generally, it may perhaps be possible to infer a range for the 'effective PLD', incorporating, but not separating, PLD and vertical positioning. But this measure of effective would be site-specific as well as species-specific and would not allow connectivity data from one area to be extrapolated to predict connectivity for that species elsewhere.

The results obtained here suggests the need for a two-pronged programme of deep-sea larval data collection if we are to use model studies to reliably estimate deep-sea larval dispersal and connectivity. Firstly, laboratory studies of larval development and behaviour focusing on the behaviours later in the larval phase - sinking ages and rates - are needed. Secondly, field observations of time-series of vertical distribution of larvae in the water column. This second is extremely challenging for many deep-sea species with small, fragile larvae. Our model predicts some retention of larvae in all Case Study sites, so positioning such time series measurements the locations of known populations could give estimates of spawning times, PLD and evolution with time of vertical distribution of larvae in the water column. Such data is currently extremely sparse, with little laboratory data on the settling phase of deep-sea species, and few field observations of vertical larval distribution (McVeigh et al. 2017; Mullineaux et al. 2005) for deep-sea species.

While we selected behaviour traits from laboratory and field observations, we have not considered whether our resulting combined behaviours are realistic, based for example on energy stores in lecithotrophic larvae. Neither have we considered the potential effects of higher temperatures near-surface reducing larval life-spans. The exact balance between the wider spreading achievable by heading to the surface for a

shorter time or remaining at depth for a longer time will depend on the local vertical temperature and velocity structures combined with the amplitude of life-shortening by increased temperatures.

We began this study trying to answer two questions to help identify whether larval behaviours are impacting their long-term spreading: Is there any evidence that any of these behaviours, either alone or combined, cause greater spreading? And, do any of these behaviours cause larvae to follow particular pathways so they settle in specific locations? Our work predicts that larval behaviours impact the long-term spreading, with wider spreading being strongly associated with more time spent higher in the water column. But the strength of this effect varies regionally (from strong to very strong). Pathways are also predicted to be affected by larval behaviour in ways which could influence the distribution of species. For example northward spread along both the eastern and western boundary appears to rely on near-surface drifting, while deep drifting strengthens the west-to-east dispersal south of Iceland.

References

Arellano, S. M., A. L. Van Gaest, S. B. Johnson, R. C. Vrijenhoek, and C. M. Young (2014). "Larvae from deep-sea methane seeps disperse in surface waters." In: *Proceedings. Biological sciences* 281.1786, p. 20133276. DOI: 10.1098/rspb.2013.3276.

Blanke, B., M. Arhan, G. Madec, S. Roche, B. Blanke, M. Arhan, G. Madec, and S. Roche (1999). "Warm Water Paths in the Equatorial Atlantic as Diagnosed with a General Circulation Model". In: *Journal of Physical Oceanography* 29.11, pp. 2753–2768. DOI: 10.1175/1520-0485(1999)029<2753:WWPITE>2.0.CO;2.

Böning, C. W., E. Behrens, A. Biastoch, K. Getzlaff, and J. L. Bamber (2016). "Emerging impact of Greenland meltwater on deepwater formation in the North Atlantic Ocean". In: *Nature Geoscience* 9.7, pp. 523–527. DOI: 10.1038/ngeo2740.

Bradbury, I. R., B. Laurel, P. V. R. Snelgrove, P. Bentzen, and S. E. Campana (2008). "Global patterns in marine dispersal estimates: the influence of geography, taxonomic category and life history." In: *Proceedings. Biological sciences* 275.1644, pp. 1803–9. DOI: 10.1098/rspb.2008.0216.

Breusing, C., A. Biastoch, A. Drews, A. Metaxas, D. Jollivet, R. C. Vrijenhoek, T. Bayer, F. Melzner, L. Sayavedra, J. M. Petersen, N. Dubilier, M. B. Schilhabel, P. Rosenstiel, and T. B. Reusch (2016). "Biophysical and Population Genetic Models Predict the Presence of "Phantom" Stepping Stones Connecting Mid-Atlantic Ridge Vent Ecosystems". In: *Current Biology* 26.17, pp. 2257–2267. DOI: 10.1016/J.CUB.2016.06.062.

Brooke, S. and C. M. Young (2005). "Embryogenesis and larval biology of the ahermatypic scleractinian Oculina varicosa". In: *Marine Biology* 146.4, pp. 665–675. DOI: 10.1007/s00227-004-1481-9.

Burgess, S. C., K. J. Nickols, C. D. Griesemer, L. A. K. Barnett, A. G. Dedrick, E. V. Satterthwaite, L. Yamane, S. G. Morgan, J. W. White, and L. W. Botsford (2014). "Beyond connectivity: How empirical methods can quantify population

persistence to improve marine protected-area design". In: *Ecological Applications* 24.2, pp. 257–270. DOI: 10.1890/13-0710.1.

Cabral, R. B., S. D. Gaines, M. T. Lim, M. P. Atrigenio, S. S. Mamauag, G. C. Pedemonte, and P. M. Aliño (2016). "Siting marine protected areas based on habitat quality and extent provides the greatest benefit to spatially structured metapopulations". In: *Ecosphere* 7.11, e01533. DOI: 10.1002/ecs2.1533.

Cetina-Heredia, P., E. van Sebille, R. J. Matear, and M. Roughan (2018). "Nitrate Sources, Supply, and Phytoplankton Growth in the Great Australian Bight: An Eulerian-Lagrangian Modeling Approach". In: *Journal of Geophysical Research: Oceans* 123.2, pp. 759–772. DOI: 10.1002/2017JC013542.

Cordes, E. E., S. L. Carney, S. Hourdez, R. S. Carney, J. M. Brooks, and C. R. Fisher (2007). "Cold seeps of the deep Gulf of Mexico: Community structure and biogeographic comparisons to Atlantic equatorial belt seep communities". In: *Deep Sea Research Part I: Oceanographic Research Papers* 54.4, pp. 637–653. DOI: 10.1016/J.DSR.2007.01.001.

Cowen, R. K. and S. Sponaugle (2009). "Larval Dispersal and Marine Population Connectivity". In: *Annu. Rev. Mar. Sci* 1.1, pp. 443–66. DOI: 10.1146/annurev.marine.010908.163757.

Dahl, M. P., R. T. Pereyra, T. Lundälv, and C. André (2012). "Fine-scale spatial genetic structure and clonal distribution of the cold-water coral Lophelia pertusa". In: *Coral Reefs* 31.4, pp. 1135–1148. DOI: 10.1007/s00338-012-0937-5.

Debreu, L., C. Vouland, and E. Blayo (2008). "AGRIF: Adaptive grid refinement in Fortran". In: *Computers & Geosciences* 34.1, pp. 8–13. DOI: 10.1016/J.CAGEO.2007.01.009.

Döös, K. (1995). "Interocean exchange of water masses". In: *Journal of Geophysical Research* 100.C7, p. 13499. DOI: 10.1029/95JC00337.

Foster, N. L. et al. (2012). "Connectivity of Caribbean coral populations: Complementary insights from empirical and modelled gene flow". In: *Molecular Ecology* 21.5, pp. 1143–1157. DOI: 10.1111/j.1365-294X.2012.05455.x.

Fox, A. D., L.-A. Henry, D. W. Corne, and J. M. Roberts (2016). "Sensitivity of marine protected area network connectivity to atmospheric variability Author for correspondence :" in: *Royal Society Open Science* 3.11. DOI: https://dx.doi.org/10.6084/m9.figshare.c.3569484.v4.

Hardesty, B. D., J. Harari, A. Isobe, L. Lebreton, N. Maximenko, J. Potemra, E. van Sebille, A. D. Vethaak, and C. Wilcox (2017). "Using Numerical Model Simulations to Improve the Understanding of Micro-plastic Distribution and Pathways in the Marine Environment". In: *Frontiers in Marine Science* 4, p. 30. DOI: 10.3389/fmars.2017.00030.

Harrison, H. B., D. H. Williamson, R. D. Evans, G. R. Almany, S. R. Thorrold, G. R. Russ, K. A. Feldheim, L. Van Herwerden, S. Planes, M. Srinivasan, M. L. Berumen, and G. P. Jones (2012). "Larval export from marine reserves and the recruitment benefit for fish and fisheries". In: *Current Biology* 22.11, pp. 1023–1028. DOI: 10.1016/j.cub.2012.04.008.

Hart-Davis, M. G., B. C. Backeberg, I. Halo, E. van Sebille, and J. A. Johannessen (2018). "Assessing the accuracy of satellite derived ocean currents by comparing observed and virtual buoys in the Greater Agulhas Region". In: *Remote Sensing of Environment* 216, pp. 735–746. DOI: 10.1016/J.RSE.2018.03.040.

Henry, L.-A., N. Frank, D. Hebbeln, C. Wienberg, L. Robinson, T. v. de Flierdt, M. Dahl, M. Douarin, C. L. Morrison, M. L. Correa, A. D. Rogers, M. Ruckelshausen, and J. M. Roberts (2014). "Global ocean conveyor lowers extinction risk in the deep sea". In: *Deep Sea Research Part I: Oceanographic Research Papers* 88, pp. 8–16. DOI: 10.1016/J.DSR.2014.03.004.

Hilário, A., A. Metaxas, S. M. Gaudron, K. L. Howell, A. Mercier, N. C. Mestre, R. E. Ross, A. M. Thurnherr, and C. M. Young (2015). "Estimating dispersal distance in the deep sea: challenges and applications to marine reserves". English. In: *Frontiers in Marine Science* 2. DOI: 10.3389/fmars.2015.00006.

James, M. K., P. R. Armsworth, L. B. Mason, and L. Bode (2002). "The structure of reef fish metapopulations: modelling larval dispersal and retention patterns." In:

Proceedings. Biological sciences / The Royal Society 269.1505, pp. 2079–2086. DOI: 10.1098/rspb.2002.2128.

Large, W. G. and S. G. Yeager (2009). "The global climatology of an interannually varying air–sea flux data set". In: *Climate Dynamics* 33.2-3, pp. 341–364. DOI: 10.1007/s00382-008-0441-3.

Larsson, A. I., J. Järnegren, S. M. Strömberg, M. P. Dahl, T. Lundälv, and S. Brooke (2014). "Embryogenesis and larval biology of the cold-water coral Lophelia pertusa." In: *PloS one* 9.7, e102222. DOI: 10.1371/journal.pone.0102222.

Lavelle, J. W., A. M. Thurnherr, J. R. Ledwell, D. J. McGillicuddy, and L. S. Mullineaux (2010). "Deep ocean circulation and transport where the East Pacific Rise at 9–10°N meets the Lamont seamount chain". In: *Journal of Geophysical Research* 115.C12, p. C12073. DOI: 10.1029/2010JC006426.

Madec, G. (2008). "NEMO Ocean Engine". In: *Note du Pôle de modélisation, Institut Pierre-Simon Laplace (IPSL)*.

McGillicuddy, D. J., J. W. Lavelle, A. M. Thurnherr, V. K. Kosnyrev, and L. S. Mullineaux (2010). "Larval dispersion along an axially symmetric mid-ocean ridge". In: *Deep Sea Research Part I: Oceanographic Research Papers* 57.7, pp. 880–892. DOI: 10.1016/J.DSR.2010.04.003.

McVeigh, D. M., D. B. Eggleston, A. C. Todd, C. M. Young, and R. He (2017). "The influence of larval migration and dispersal depth on potential larval trajectories of a deep-sea bivalve". In: *Deep Sea Research Part I: Oceanographic Research Papers* 127, pp. 57–64. DOI: 10.1016/J.DSR.2017.08.002.

Mullineaux, L. S., S. W. Mills, A. K. Sweetman, A. H. Beaudreau, A. Metaxas, and H. L. Hunt (2005). "Vertical, lateral and temporal structure in larval distributions at hydrothermal vents". In: *Marine Ecology Progress Series* 293, pp. 1–16. DOI: 10.3354/meps293001.

Olds, A. D., R. M. Connolly, K. A. Pitt, and P. S. Maxwell (2012). "Habitat connectivity improves reserve performance". In: *Conservation Letters* 5.1, pp. 56–63. DOI: 10.1111/j.1755-263X.2011.00204.x.

Planes, S., G. P. Jones, and S. R. Thorrold (2009). "Larval dispersal connects fish populations in a network of marine protected areas." In: *Proceedings of the National Academy of Sciences of the United States of America* 106.14, pp. 5693–7. DOI: 10.1073/pnas.0808007106.

Ross, R. E., W. A. M. Nimmo-Smith, and K. L. Howell (2016). "Increasing the Depth of Current Understanding: Sensitivity Testing of Deep-Sea Larval Dispersal Models for Ecologists". In: *PLOS ONE* 11.8. Ed. by A. Davies, e0161220. DOI: 10.1371/journal.pone.0161220.

Sebille, E. van et al. (2018). "Lagrangian ocean analysis: Fundamentals and practices". In: *Ocean Modelling* 121, pp. 49–75. DOI: 10.1016/J.OCEMOD.2017.11.008.

Soest, R. van and N. de Voogd (2015). "Sponge species composition of north-east Atlantic cold-water coral reefs compared in a bathyal to inshore gradient". In: *Journal of the Marine Biological Association of the United Kingdom* 95.07, pp. 1461–1474. DOI: 10.1017/S0025315413001410.

Strömberg, S. M. and A. I. Larsson (2017). "Larval Behavior and Longevity in the Cold-Water Coral Lophelia pertusa Indicate Potential for Long Distance Dispersal". In: *Frontiers in Marine Science* 4, p. 411. DOI: 10.3389/fmars.2017.00411.

Teske, P. R., J. Sandoval-Castillo, E. van Sebille, J. Waters, and L. B. Beheregaray (2016). "Oceanography promotes self-recruitment in a planktonic larval disperser". In: *Scientific Reports* 6.1, p. 34205. DOI: 10.1038/srep34205.

Truelove, N. K., A. S. Kough, D. C. Behringer, C. B. Paris, S. J. Box, R. F. Preziosi, and M. J. Butler (2017). "Biophysical connectivity explains population genetic structure in a highly dispersive marine species". In: *Coral Reefs* 36.1, pp. 233–244. DOI: 10.1007/s00338-016-1516-y.

Wang, T., S. T. Gille, M. R. Mazloff, N. V. Zilberman, Y. Du, T. Wang, S. T. Gille, M. R. Mazloff, N. V. Zilberman, and Y. Du (2018). "Numerical Simulations to Project Argo Float Positions in the Middepth and Deep Southwest Pacific".

In: *Journal of Atmospheric and Oceanic Technology* 35.7, pp. 1425–1440. DOI: 10.1175/JTECH-D-17-0214.1.

Yearsley, J. M. and J. D. Sigwart (2011). "Larval Transport Modeling of Deep-Sea Invertebrates Can Aid the Search for Undiscovered Populations". In: *PLoS ONE* 6.8. Ed. by P. Roopnarine, e23063. DOI: 10.1371/journal.pone.0023063.

Young, C. M., R. He, R. B. Emlet, Y. Li, H. Qian, S. M. Arellano, A. Van Gaest, K. C. Bennett, M. Wolf, T. I. Smart, and M. E. Rice (2012). "Dispersal of Deep-Sea Larvae from the Intra-American Seas: Simulations of Trajectories using Ocean Models". In: *Integrative and Comparative Biology* 52.4, pp. 483–496. DOI: 10.1093/icb/ics090.

	Case Study Name	bathy min. [m]	bathy max. [m]	particles per launch	notes
1	LoVe Observatory	20	2000	1683	added points
2	Western Scottish Slope	400	600	259	
3	Rockall Bank	200	2000	4508	every 4th node
4	Mingalay Reef	100	200	729	added points
5	Porcupine Seabight	200	1200	5295	
6	Bay of Biscay	200	2000	1339	
7	Gulf of Cádiz/Alboran Sea	30	2200	1764	
8	Azores	150	1250	1968	
9	Reykjanes Ridge	200	2000	1917	every 10th node
10	Davis Strait	200	2000	950	
11	Flemish Cap	600	1450	2349	
12	US Mid-Atlantic Canyons	200	1500	302	

Table 1: Numbers of particles representing each Case Study (CS) at each release time. These numbers are the number of particles in each release ensemble. For each release time, one particle was released at every VIKING20 bottom grid node that lies within the CS polygon and the given isobath range (i.e. the red dots in Figure 1). Particles were released at 200 discrete times: one burst of particles in the middle of each season over 50 years of the model run from 1959 to 2008. The middle of each season is defined as mid-January, mid-April, mid-July, and mid-October. Taking into account that particles were also released near the very bottom and top of each grid box, the total number of particles simulated for each CS (the total ensemble) is the number in the fifth column times 400 (400 = 50 years times 4 seasons per year times 2 launch depths). Polygons for CS01 and CS04 only encompassed a small number of model grid points, 187 and 9, respectively, so additional particles were added to the simulations by creating new particles offset by ± 0.3 index units (for both) and ± 0.1 index units (only for CS04) to the particles launched exactly at the grid nodes. CS03 and CS09 polygons contained too many points so the numbers of particles for those CS were cut down by sub-sampling the number of grid nodes at which particles were released.

Behaviour index	early maturity	early competency	fast ascent	fast descent	deeper drift	linestyle
1	1	1	1	1	1	
2	1	1	1	1	0	
3	1	1	1	0	1	
4	1	1	1	0	0	
5	1	1	0	1	1	
6	1	1	0	1	0	
7	1	1	0	0	1	
8	1	1	0	0	0	
9	1	0	1	1	1	
10	1	0	1	1	0	
11	1	0	1	0	1	
12	1	0	1	0	0	
13	1	0	0	1	1	
14	1	0	0	1	0	
15	1	0	0	0	1	
16	1	0	0	0	0	
17	0	1	1	1	1	
18	0	1	1	1	0	
19	0	1	1	0	1	
20	0	1	1	0	0	
21	0	1	0	1	1	
22	0	1	0	1	0	
23	0	1	0	0	1	
24	0	1	0	0	0	
25	0	0	1	1	1	
26	0	0	1	1	0	
27	0	0	1	0	1	
28	0	0	1	0	0	
29	0	0	0	1	1	
30	0	0	0	1	0	
31	0	0	0	0	1	
32	0	0	0	0	0	

Table 2: Key to particle behaviours and the linestyles which represent them in Figure 2 and Figures 3 to 14. A '1' in the column indicates the behaviour in the header, a '0' indicates its alternative behaviour. Early(late) maturity: 0(10) days. Early(late competency): 4(42) days. Fast(slow) ascent or descent: 1.0(0.2) $\mathrm{mm\,s^{-1}}$. Deeper(shallower) drift: 120(6) m. Line styles are based around behaviour types (red – early competency, blue – slow ascent, dotted – deeper drift, dashed – late maturity, pale – fast descent) and are cumulative so purple (blue + red), dotdash (dot + dash) represents early competency, slow ascent, deeper drift and late maturity.

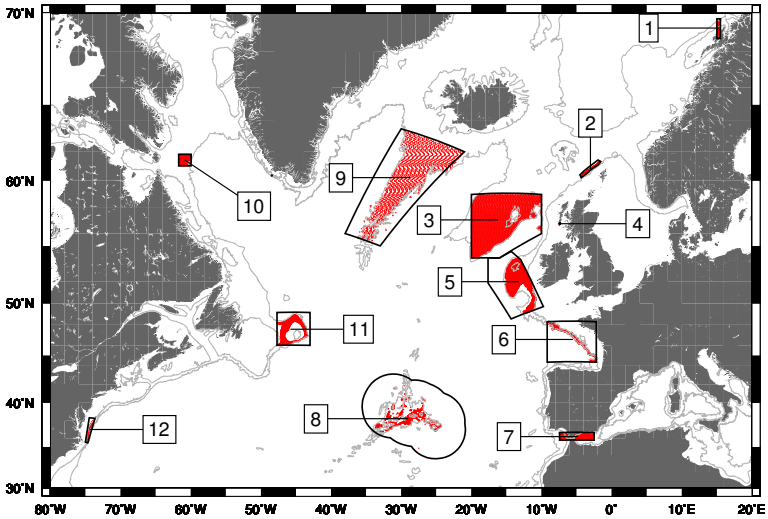

Figure 1: Map of the ATLAS Case Studies with the numbers in boxes corresponding to the left column of Table 1 (from ATLAS D1.1). Case Study polygons are shown with black lines and particle release locations are shown with red dots. The 200 m and 2000 m isobaths are shown with gray lines. Closed isobath contours with a small number of points are omitted for clarity.

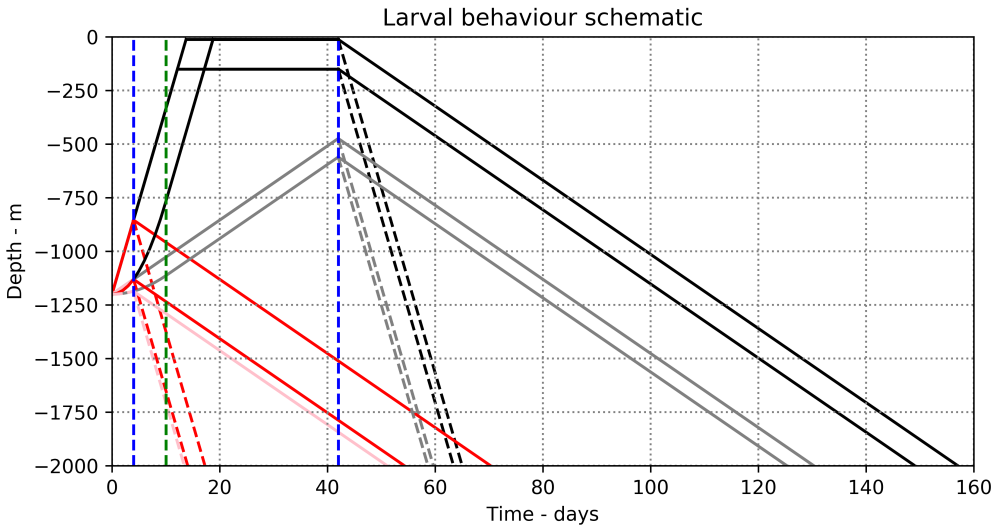

Figure 2: Larval vertical behaviour schematic showing profiles for example larvae released at 1200 m depth, showing the effects of age of maturity, age of competency, upward and downward swimming speeds and drifting target depth on vertical position. All larvae are tracked to age 185 days, larvae which reach the bed before 185 days are free to drift in the deepest model layers. Green vertical line – 10-day maturity ages (0-day maturity age not shown), blue vertical lines – early (4-day) and late (42-day) competency ages. Black/Red lines show behaviours with late/early competency, solid/dashed lines show behaviours with slow/rapid descent, and dark/pale lines show rapid/slow ascent. Some different behaviour schemes may result in identical profiles (for example if the target drifting depth is not reached before competency, and therefore descent).

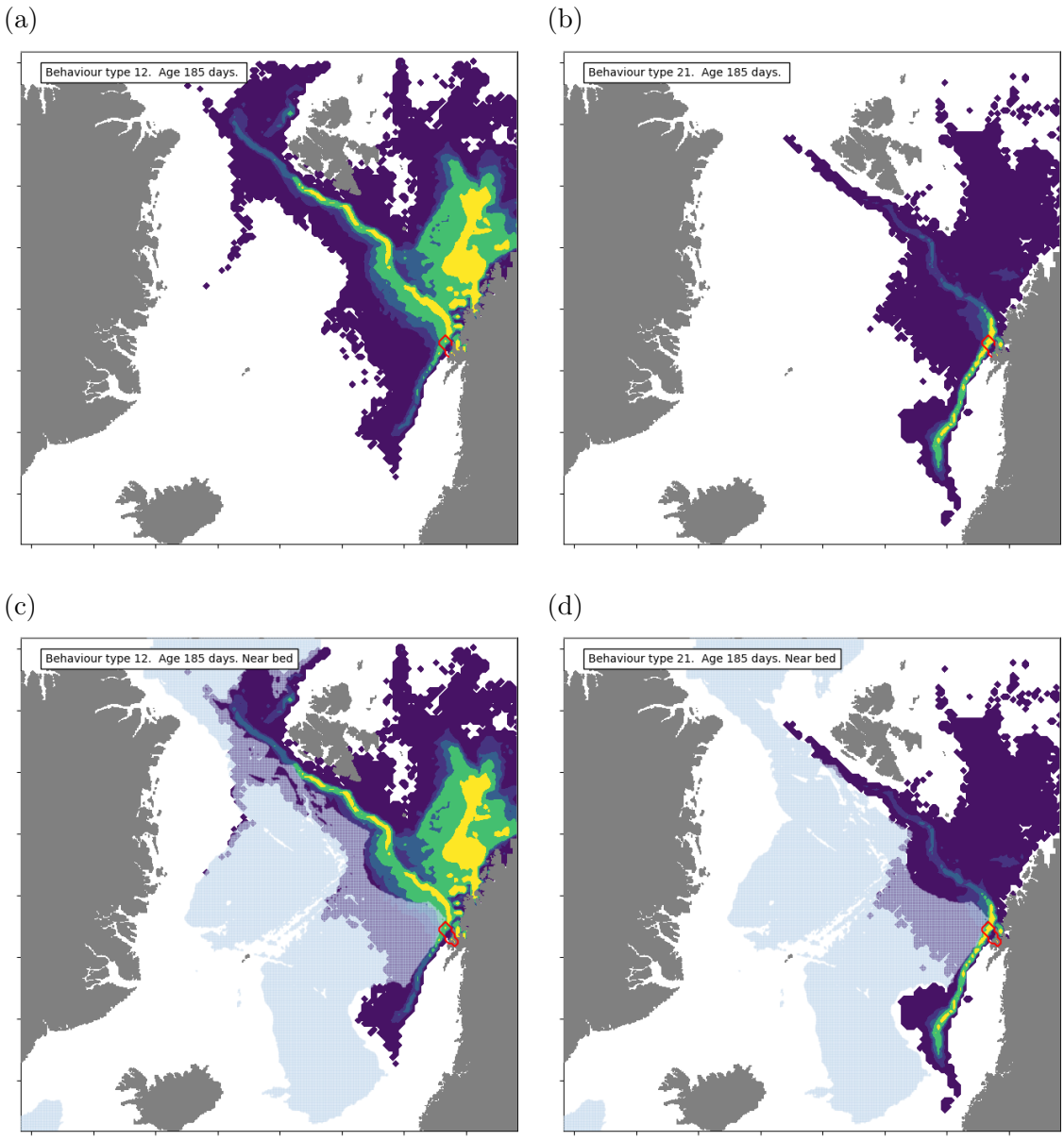

Figure 3: Case Study 01, LoVe: (a) and (b): 2D histograms showing the extent of larval dispersal after 185 days for (a): behaviour type 12 – longest period near-surface, and (b) behaviour type 21 – shortest period above bed. Colours: Yellow – area spanned by the 50% of the tracked particles in the densest part of the distribution, green – 80%, paler to darker blue – 90%, 95%, and 100%.(c) and (d): As for (a) and (b) except particles which have not returned to the bed are excluded (considered lost). Pale blue shading shows regions over 2300 m deep, where conditions are generally unsuitable for the species being considered in ATLAS. Particles were released from within the red polygon.

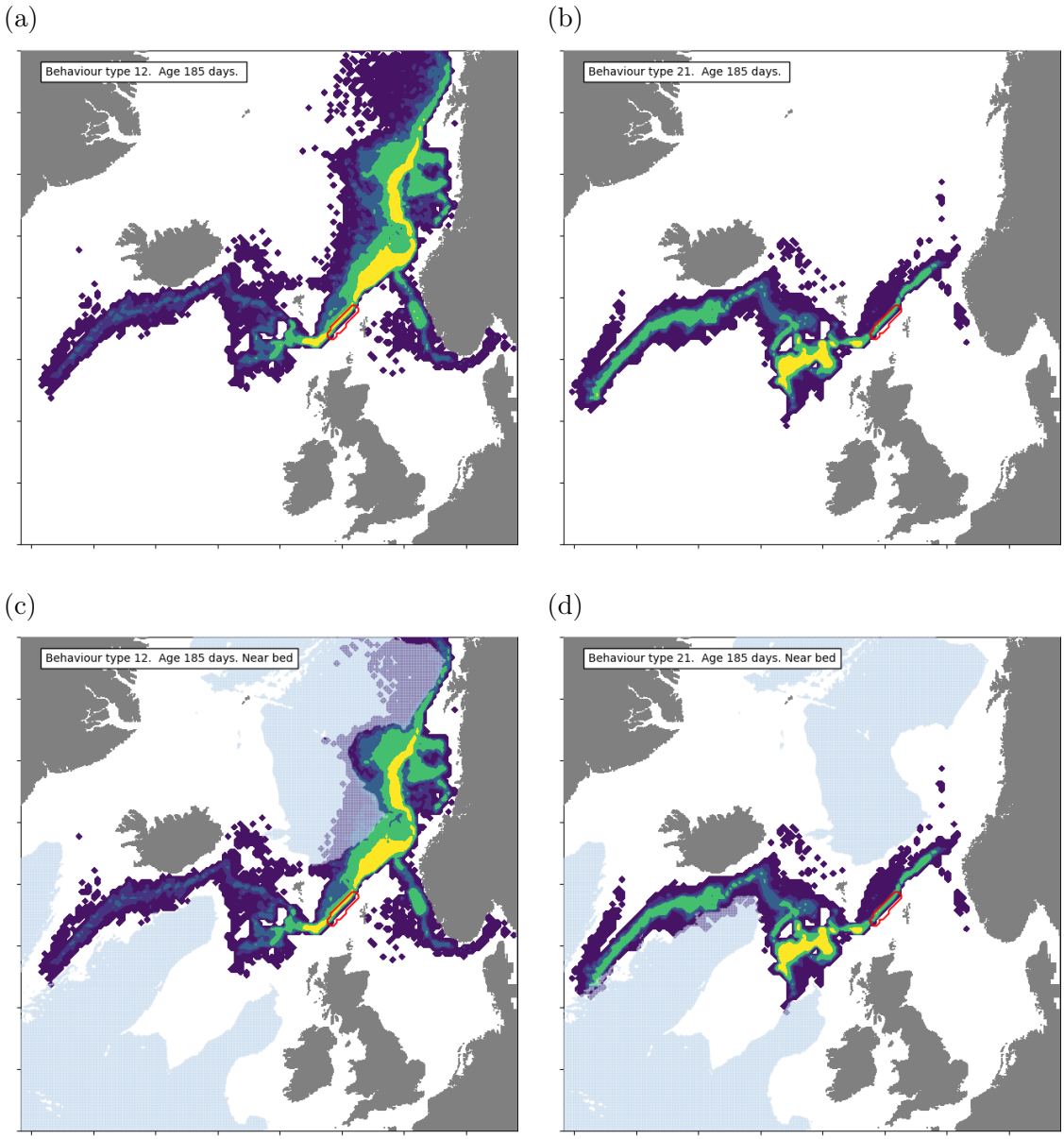

Figure 4: As Figure 3 but for Case Study 02, West Shetland Shelf.

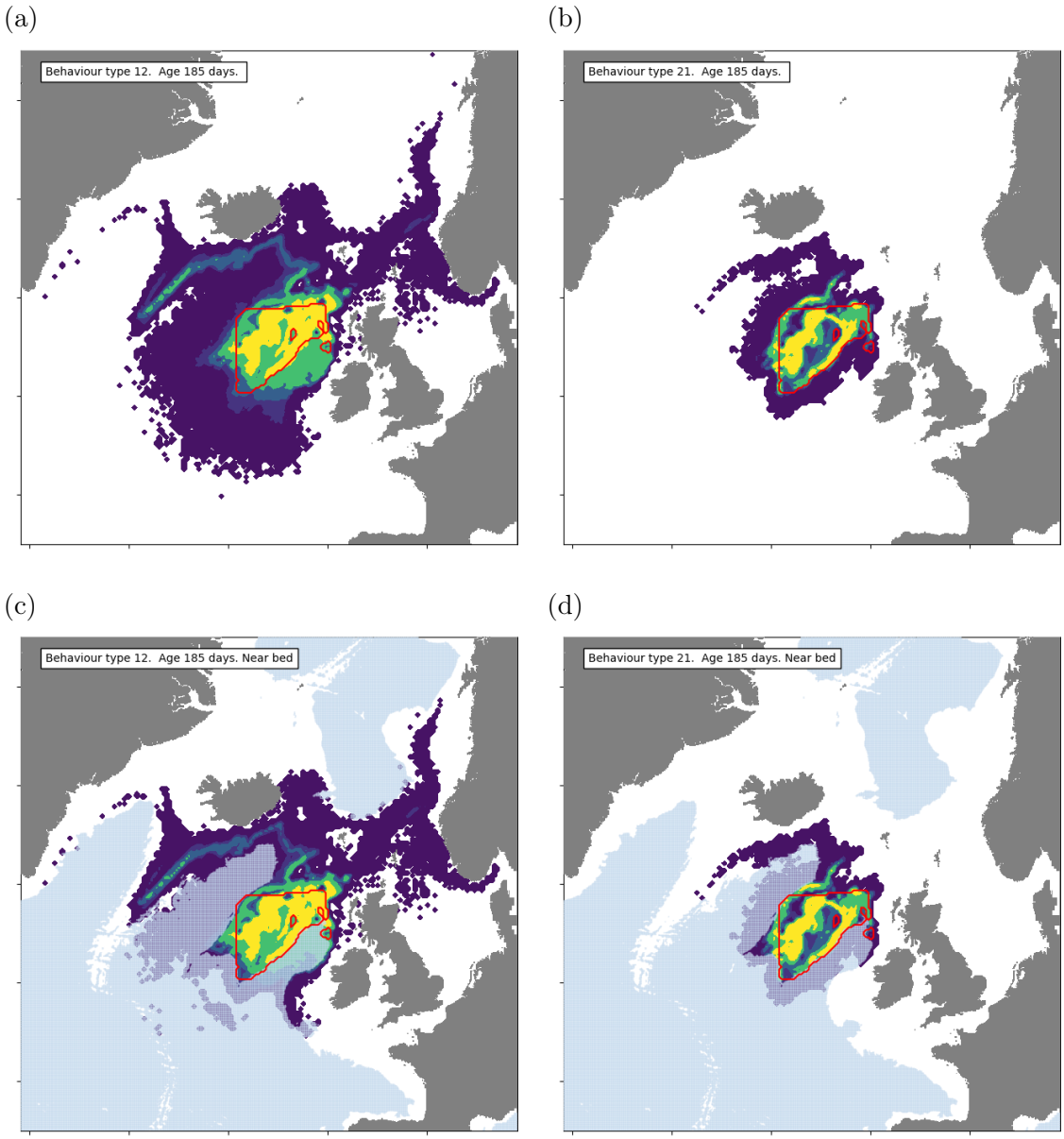

Figure 5: As Figure 3 but for Case Study 03, Rockall Bank.

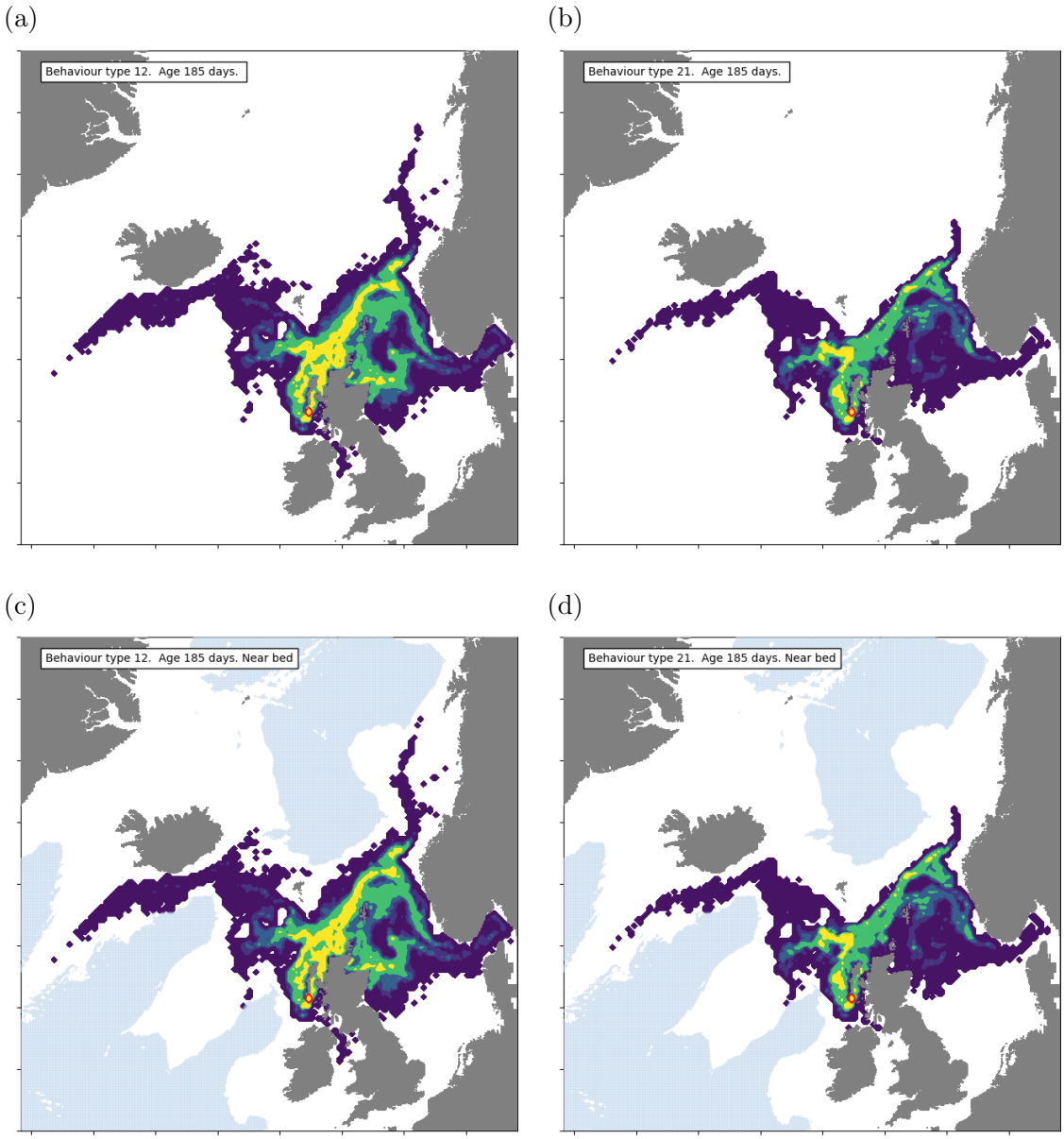

Figure 6: As Figure 3 but for Case Study 04, Mingulay.

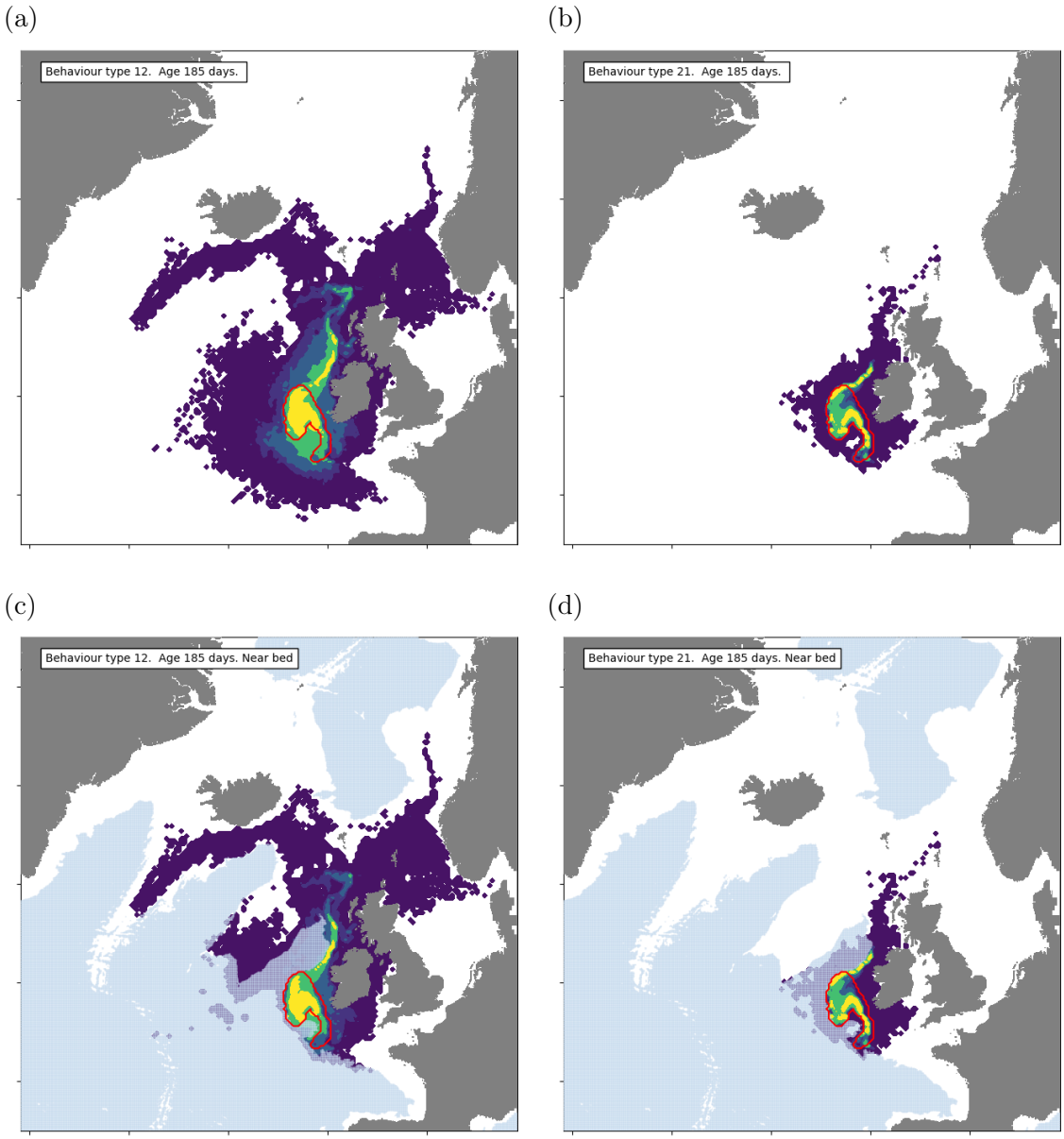

Figure 7: As Figure 3 but for Case Study 05, Porcupine Seabight.

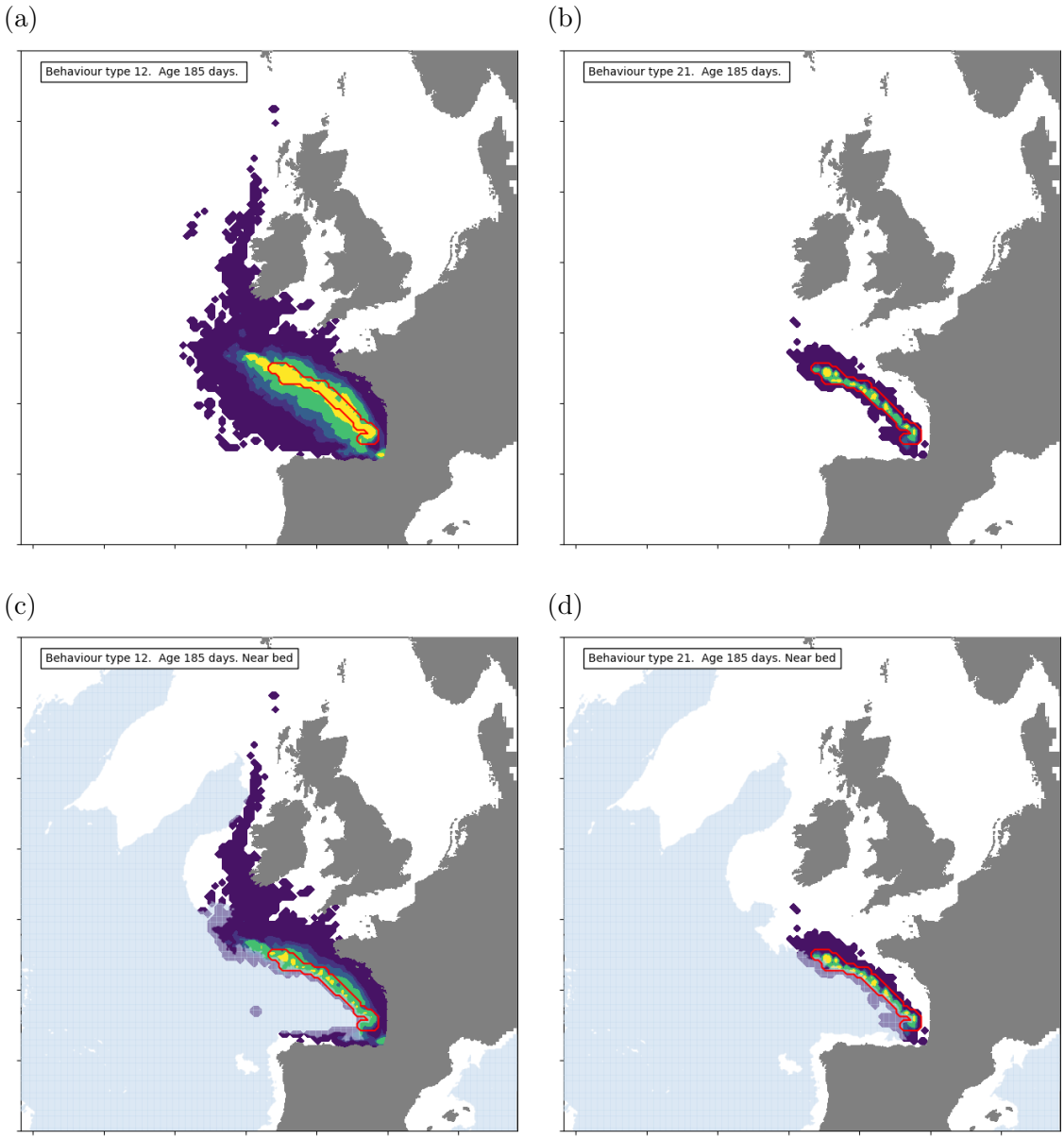

Figure 8: As Figure 3 but for Case Study 06, Bay of Biscay

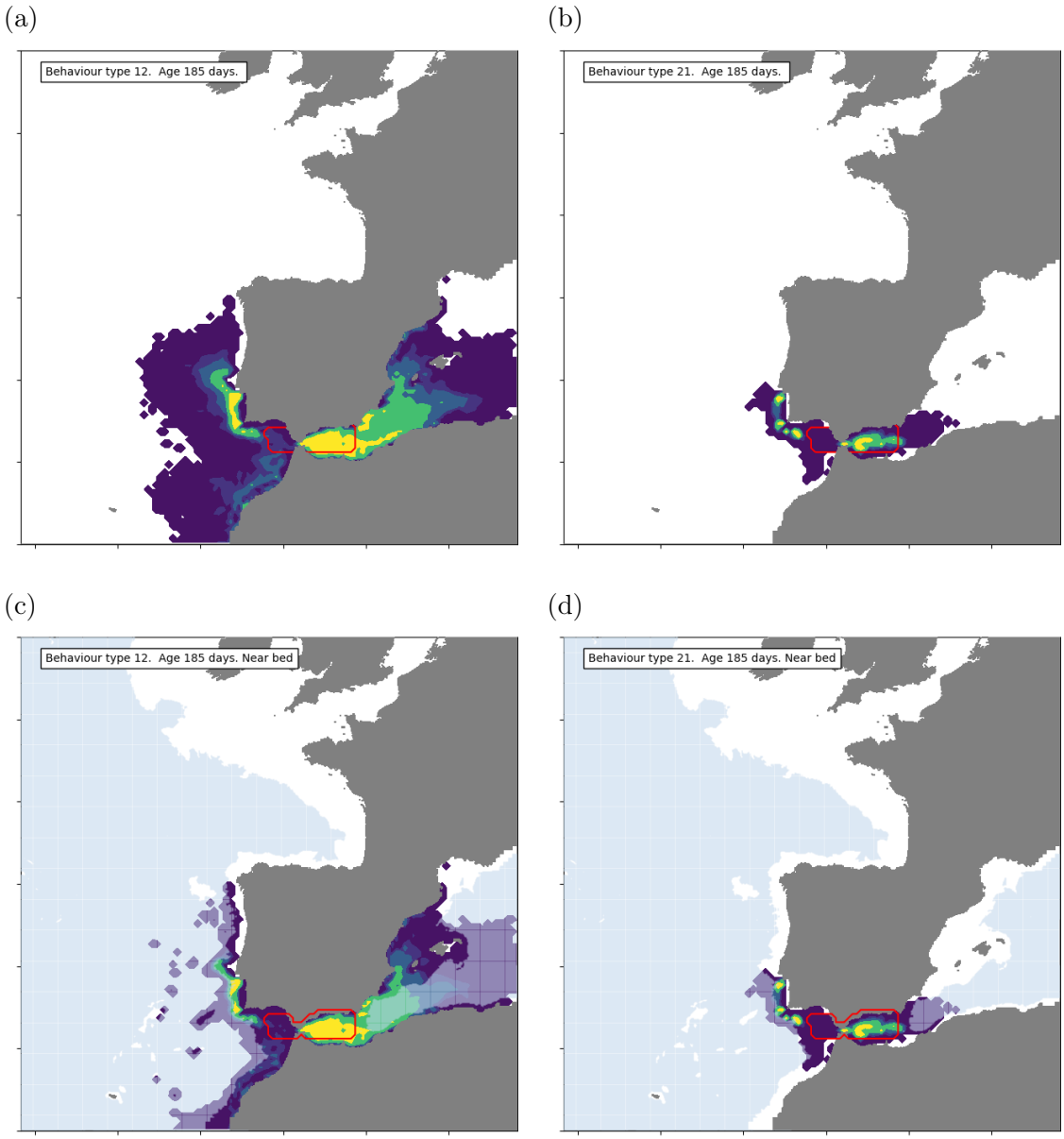

Figure 9: As Figure 3 but for Case Study 07, Gulf of Cádiz and Alboran Sea.

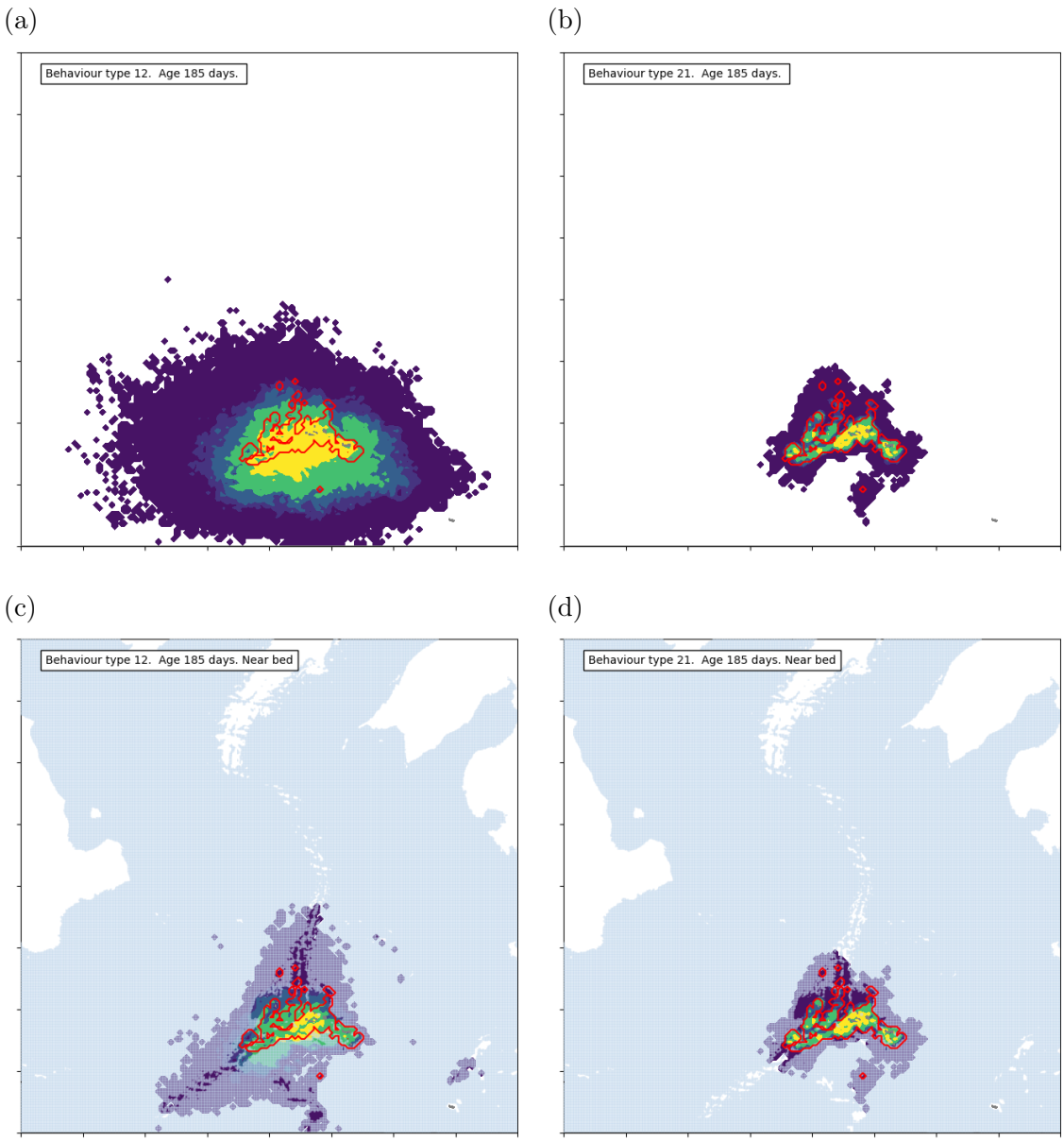

Figure 10: As Figure 3 but for Case Study 08, Azores.

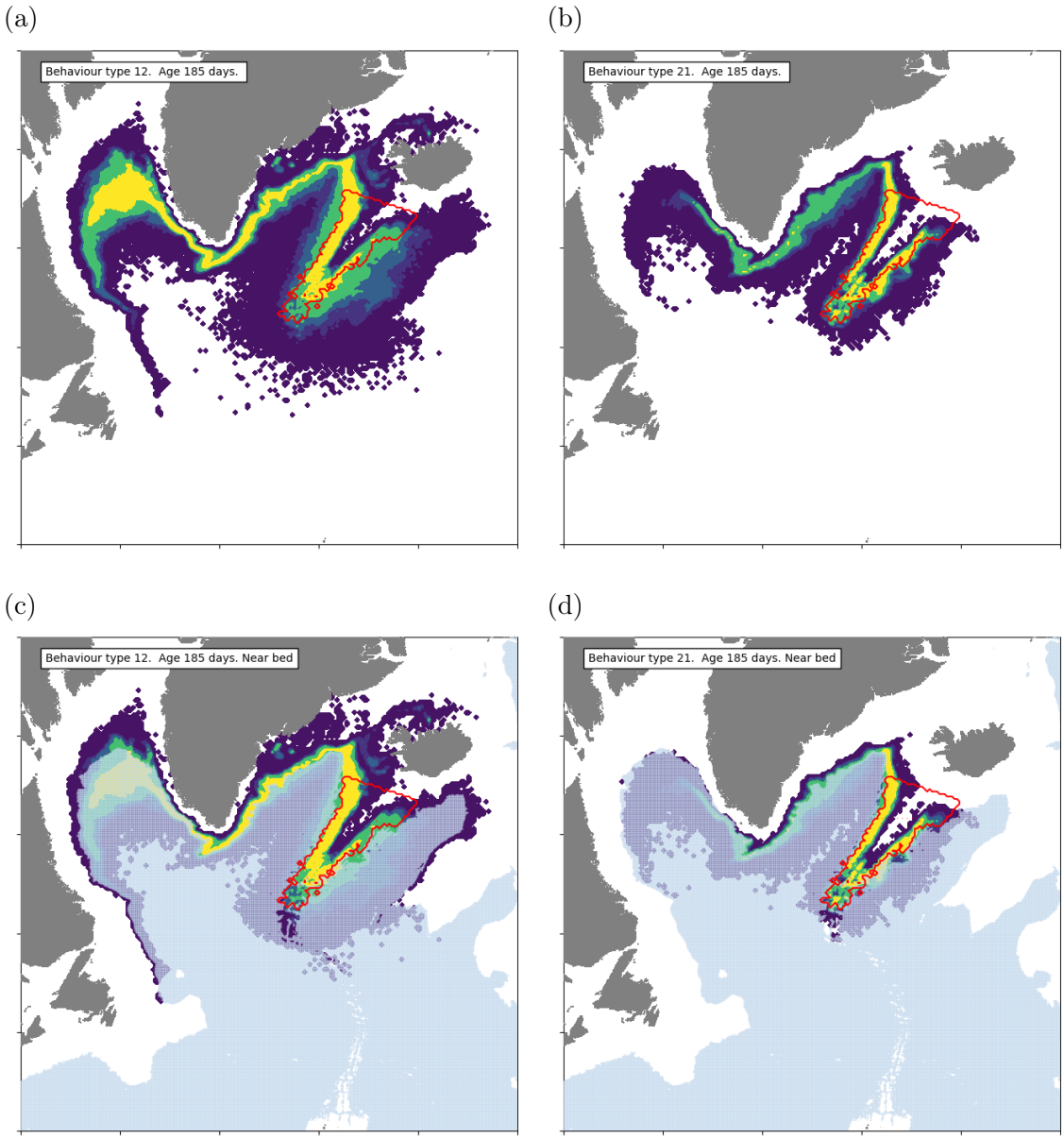

Figure 11: As Figure 3 but for Case Study 09, Reykjanes Ridge.

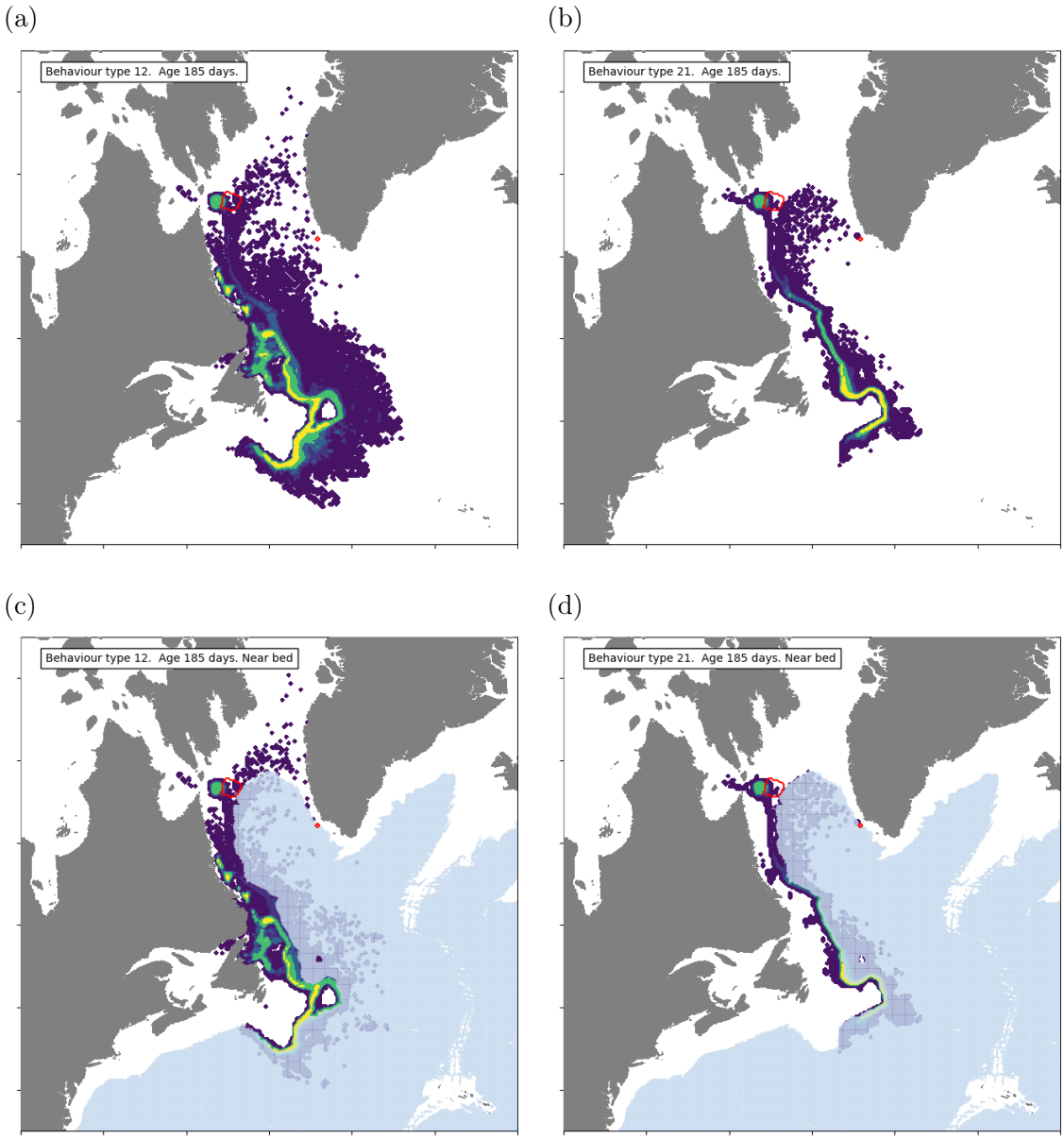

Figure 12: As Figure 3 but for Case Study 10, Davis Strait.

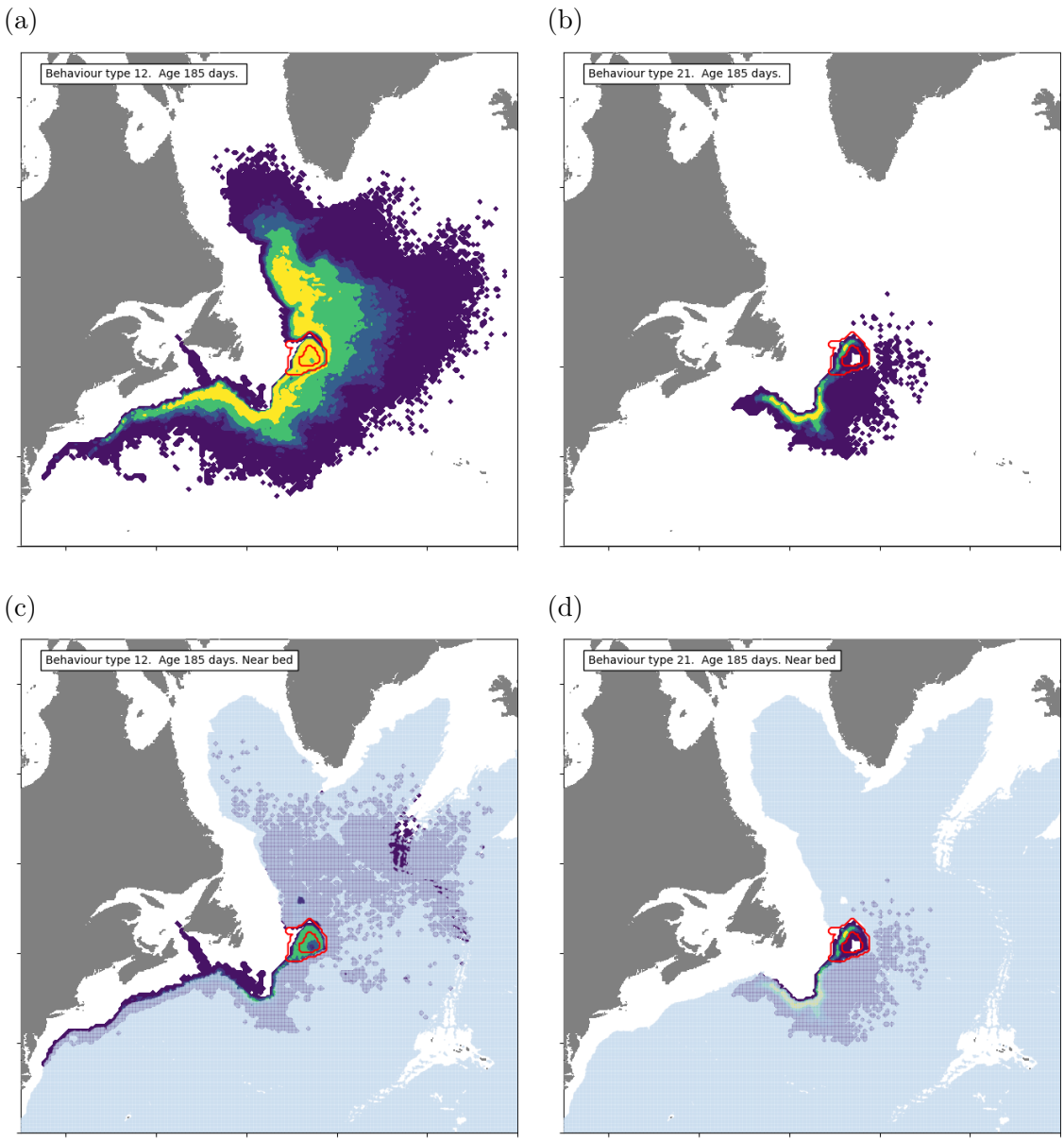

Figure 13: As Figure 3 but for Case Study 11, Flemish Cap

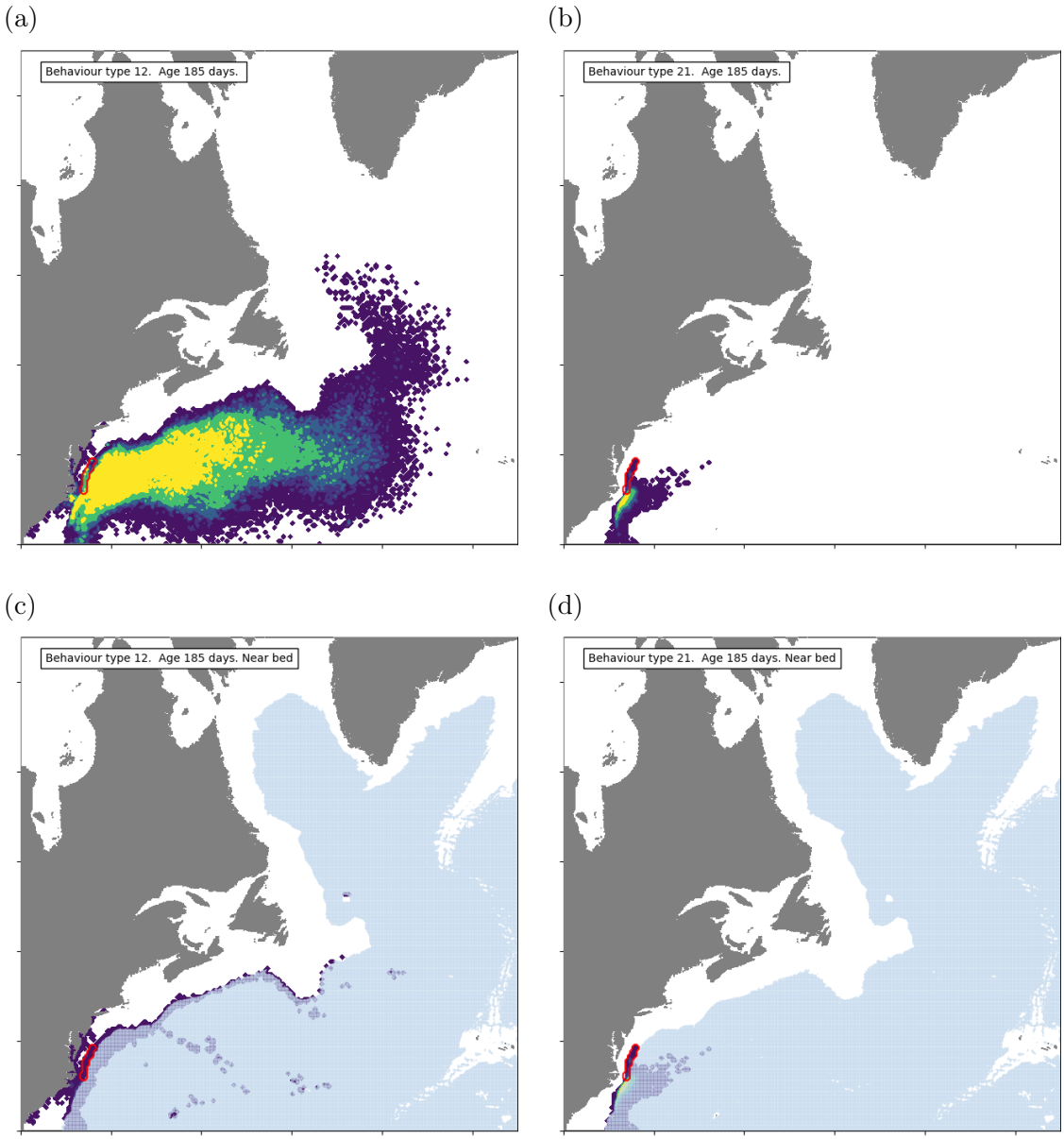

Figure 14: As Figure 3 but for Case Study 12, US Mid-Atlantic Canyons

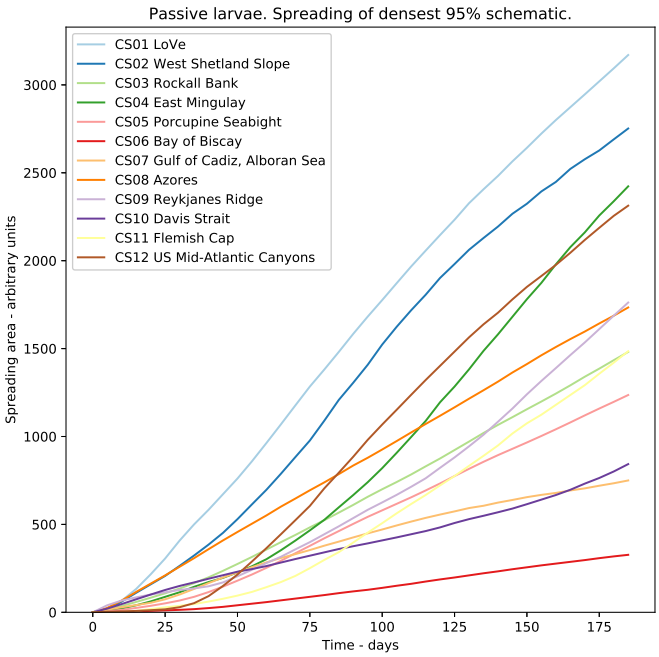

Figure 15: Change in area covered by the densest 95% of the larval distribution with time for the passive larvae runs presented in ATLAS Deliverable D1.1 (https://doi.org/10.5281/zenodo.570588). Note the dominance of linear increase in spreading area with time. Also note the different spreading rates for different Case Study regions, due to the different dynamical regimes.

(a)

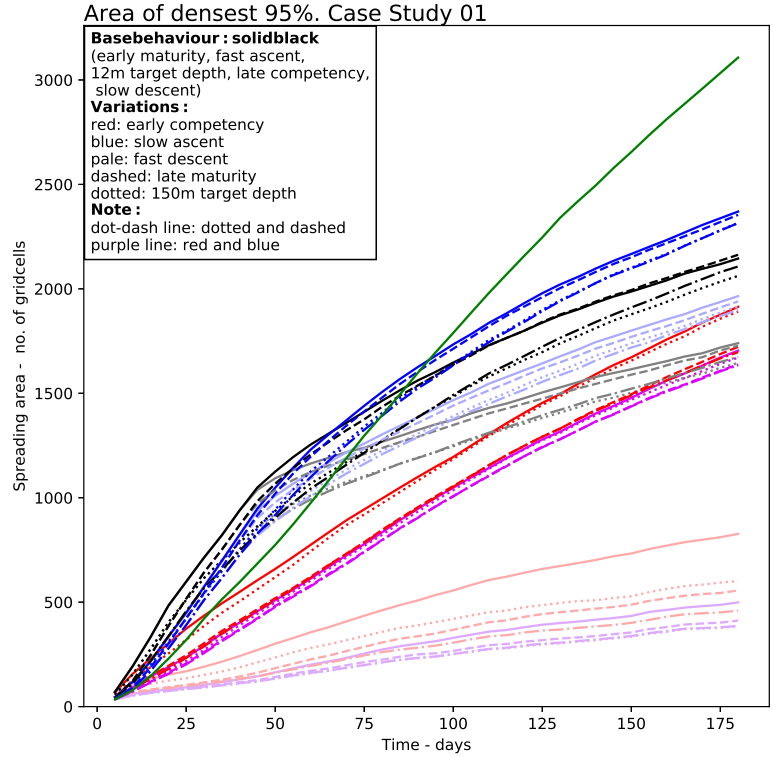

(b)

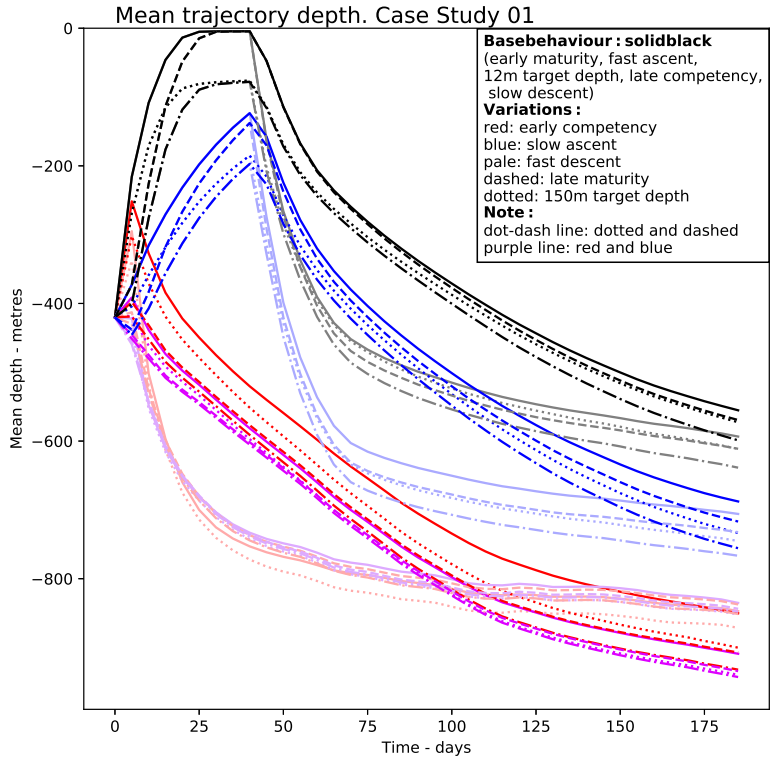

Figure 16: Case Study 01. (a) Minimum area, in model 0.25° squares, enclosing 95% of particles vs. time. (b) Average depth below surface vs. time. Lines are coloured and styled cumulatively by behaviour (see also Table 2 for key): base solid black, + red – early competence, + blue – slow ascent, + pale – fast descent, + dashes – late maturity, + dots – deeper (120 m target level). Green line in (a) represents passive particles, these passive particles do not descend to the bed so more rapid spreading continues throughout.

(a)

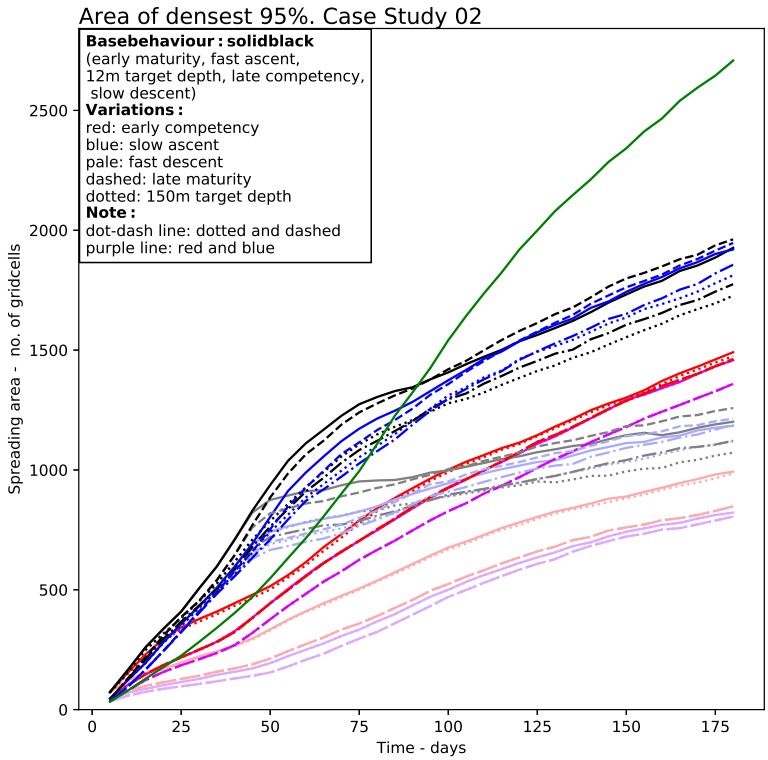

(b)

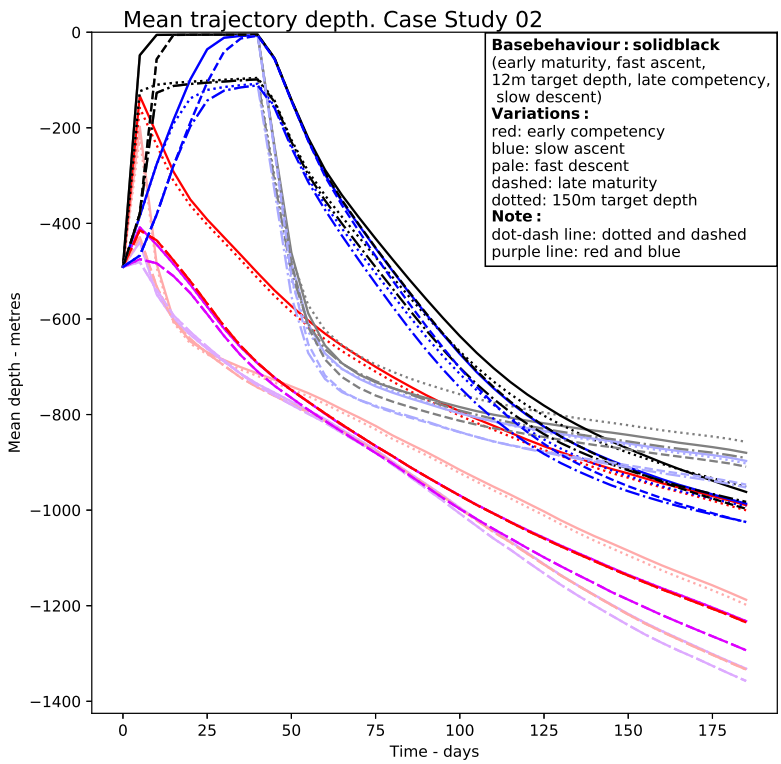

Figure 17: As Figure 16 but for Case Study 02, West Shetland Shelf.

(a)

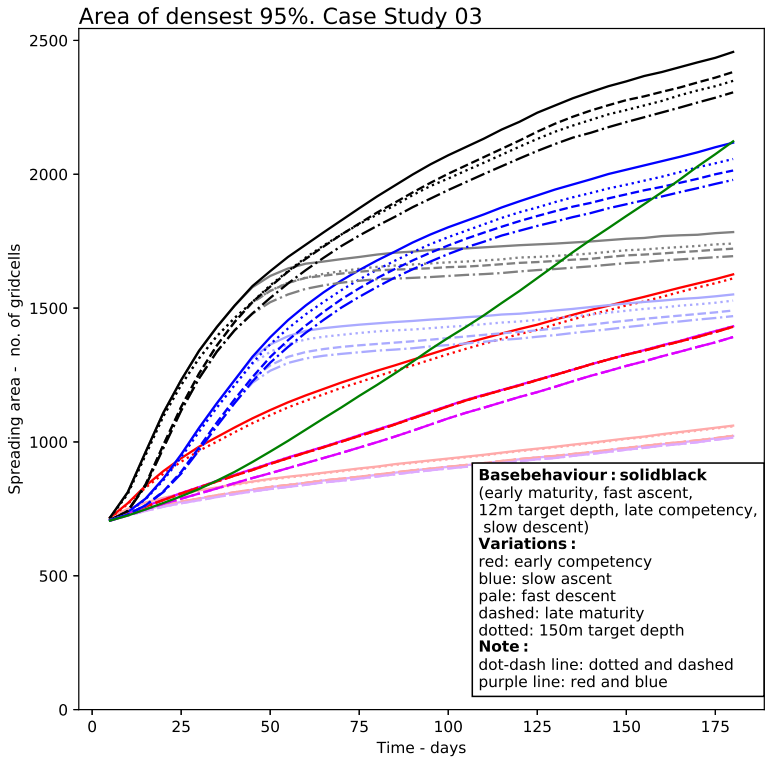

(b)

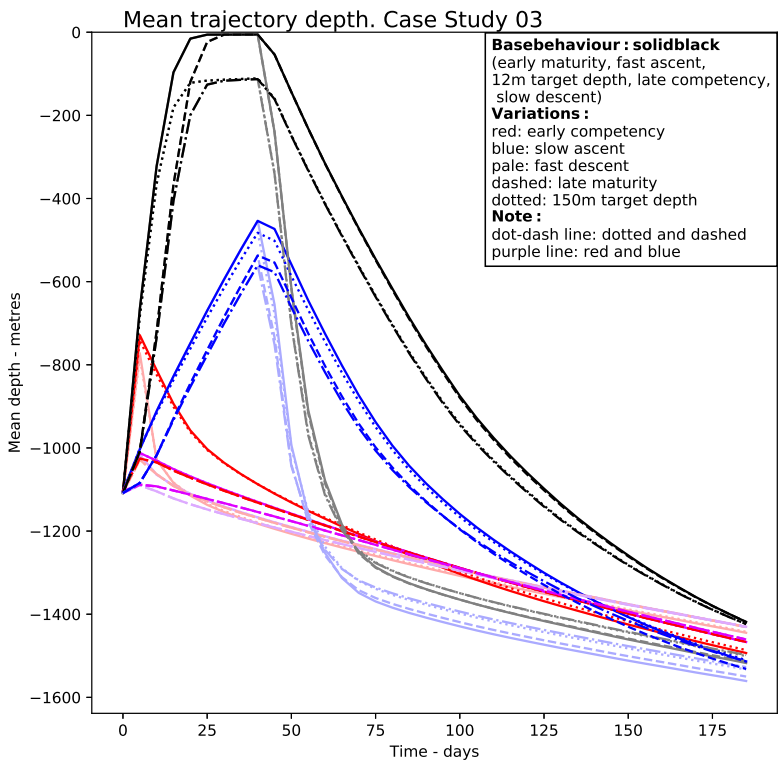

Figure 18: As Figure 16 but for Case Study 03, Rockall Bank.

(a)

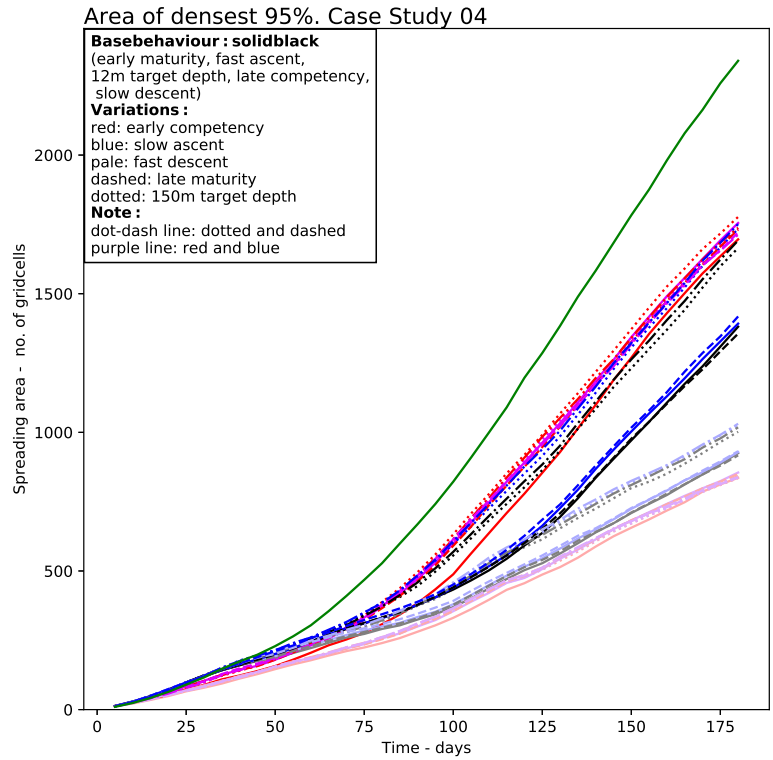

(b)

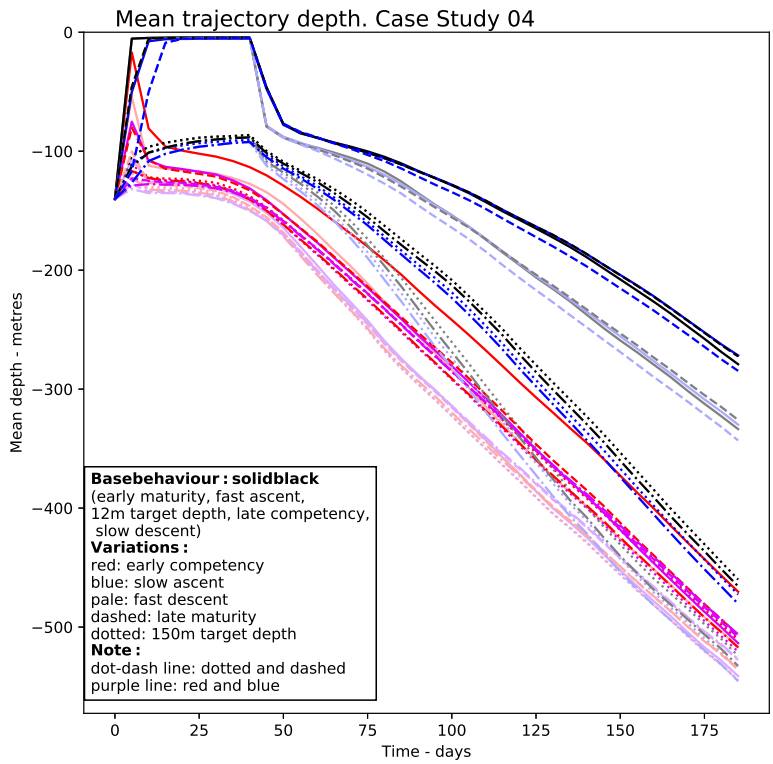

Figure 19: As Figure 16 but for Case Study 04, Mingulay.

(a)

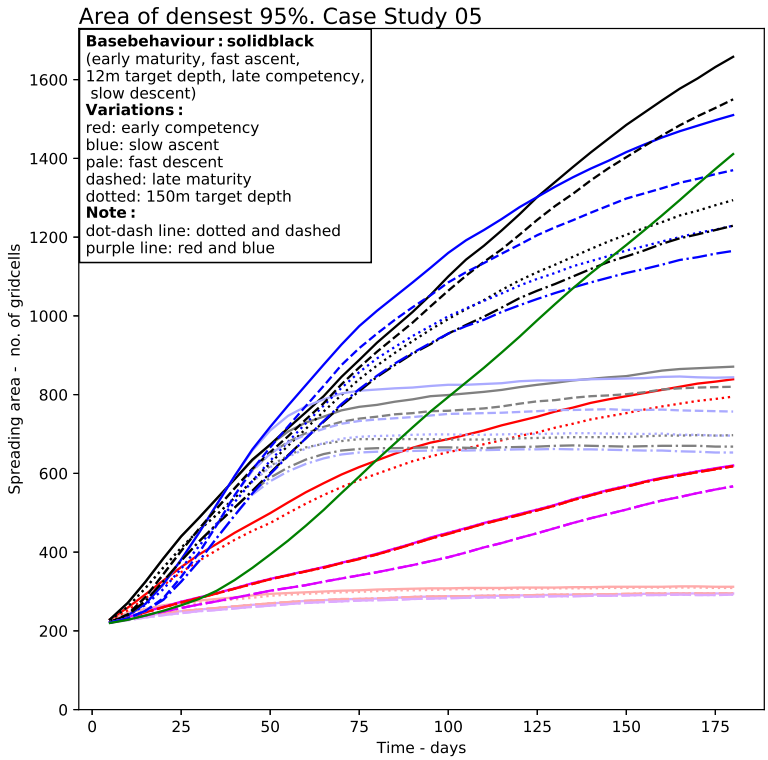

(b)

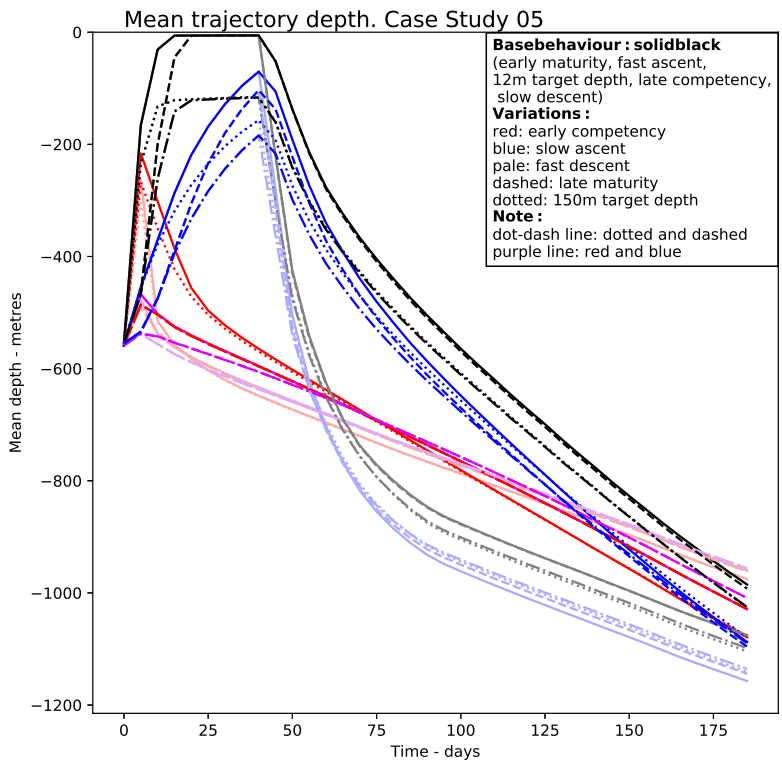

Figure 20: As Figure 16 but for Case Study 05, Porcupine Seabight.

(a)

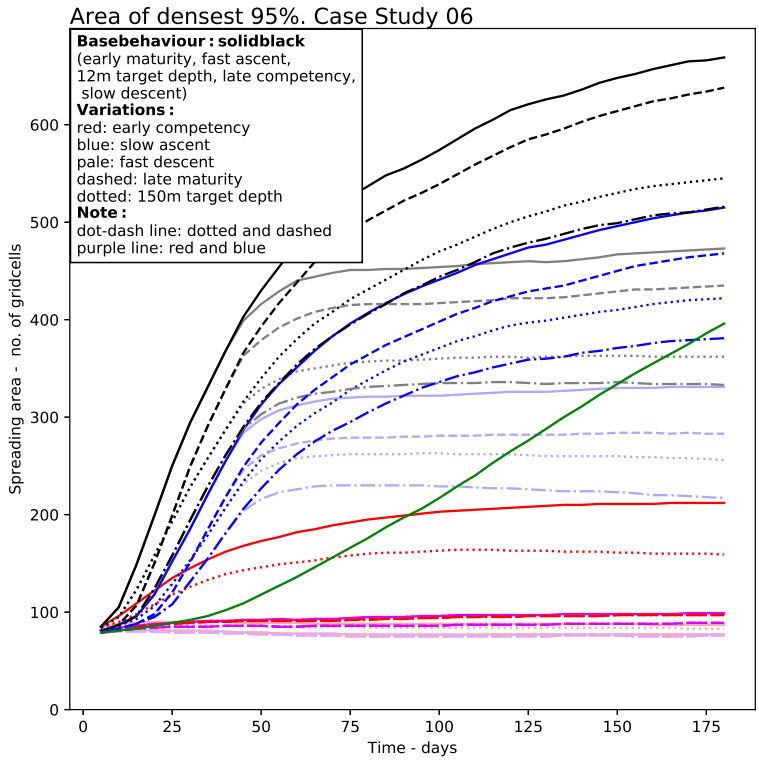

(b)

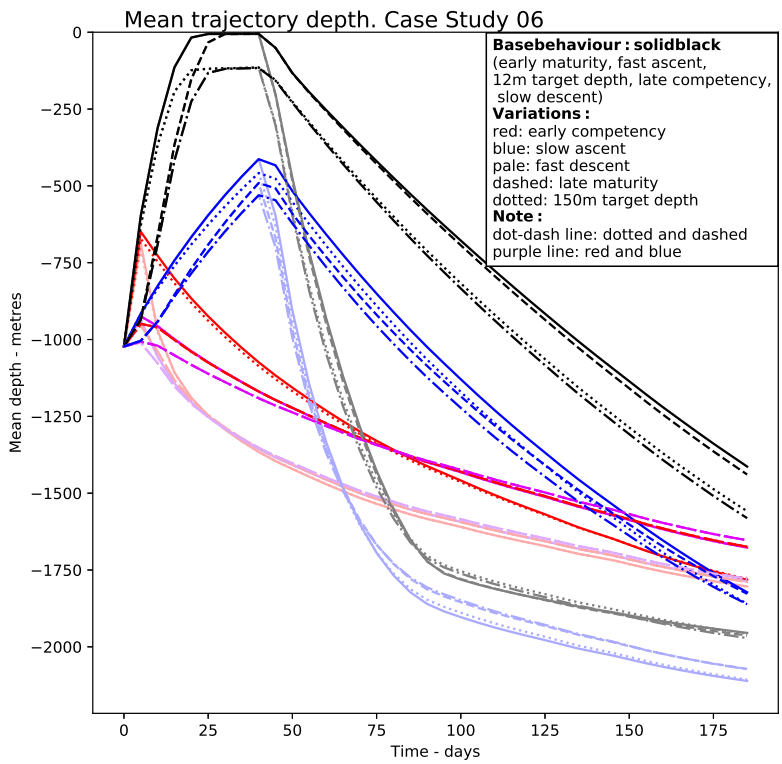

Figure 21: As Figure 16 but for Case Study 06, Bay of Biscay

(a)

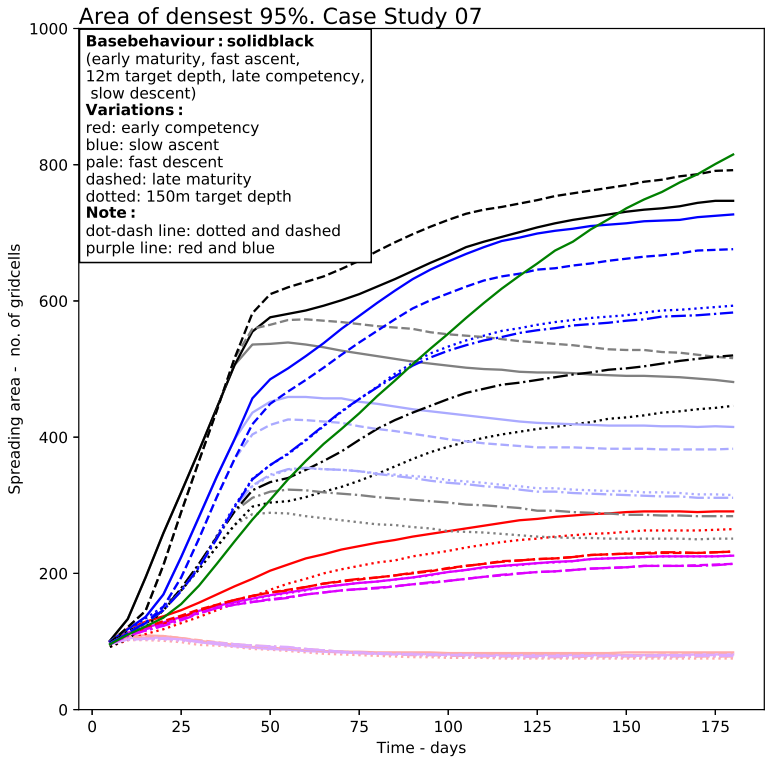

(b)

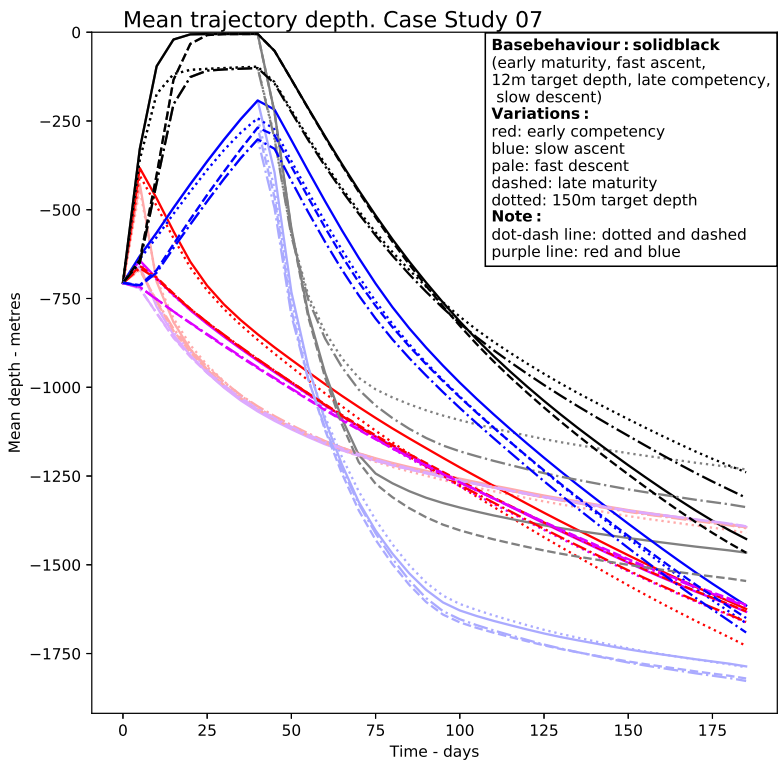

Figure 22: As Figure 16 but for Case Study 07, Gulf of Cádiz and Alboran Sea.

(a)

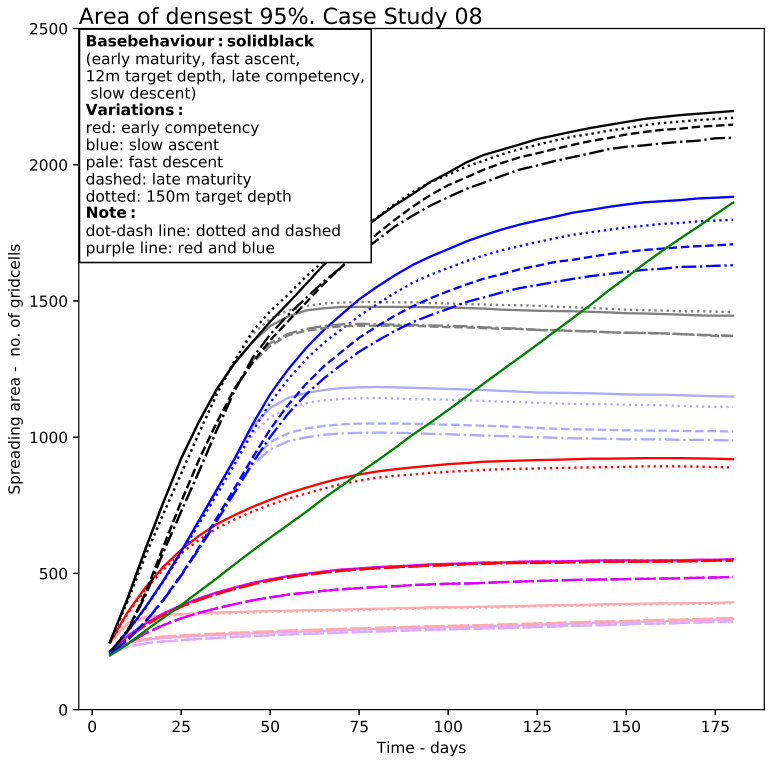

(b)

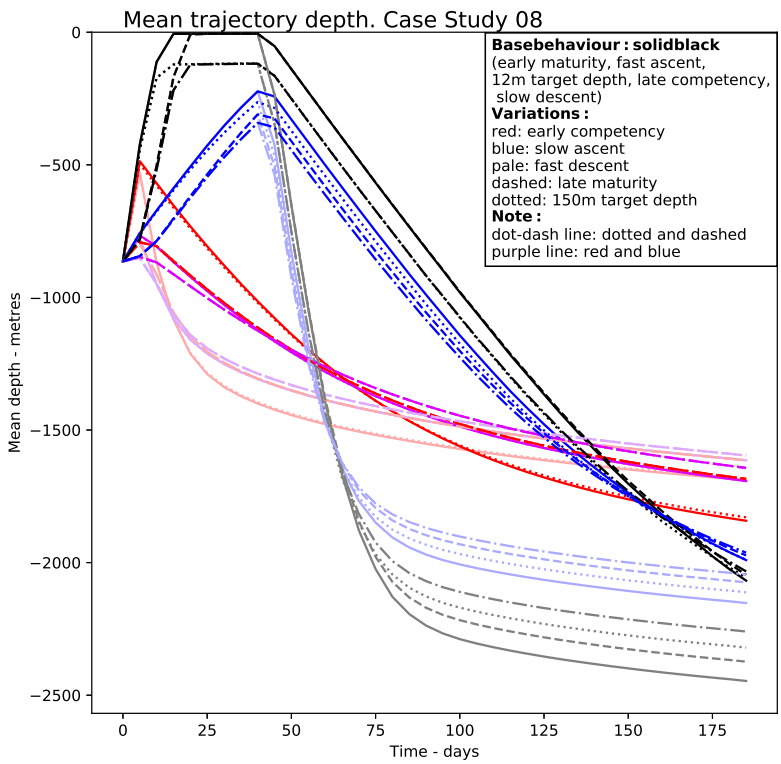

Figure 23: As Figure 16 but for Case Study 08, Azores.

(a)

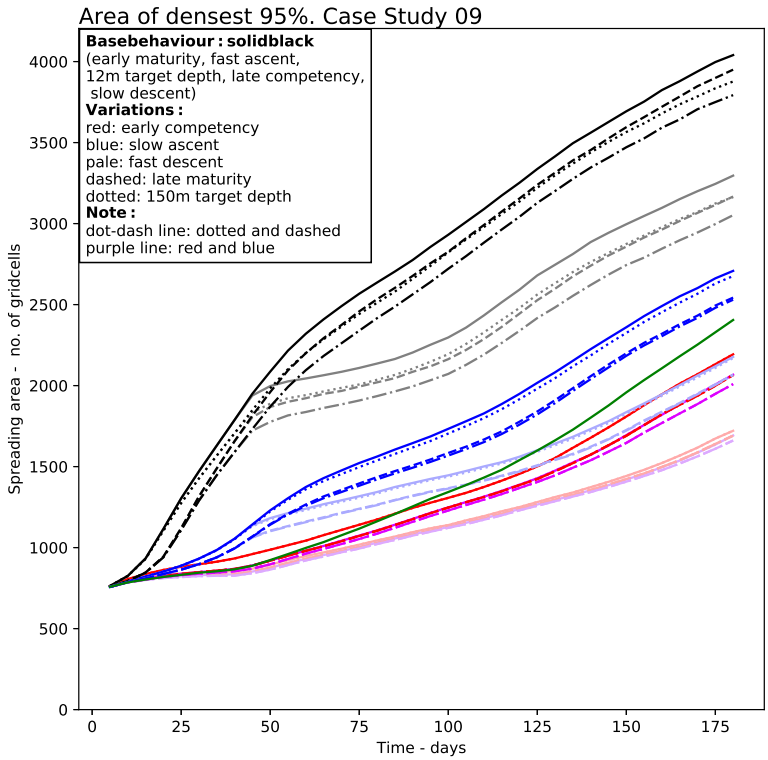

(b)

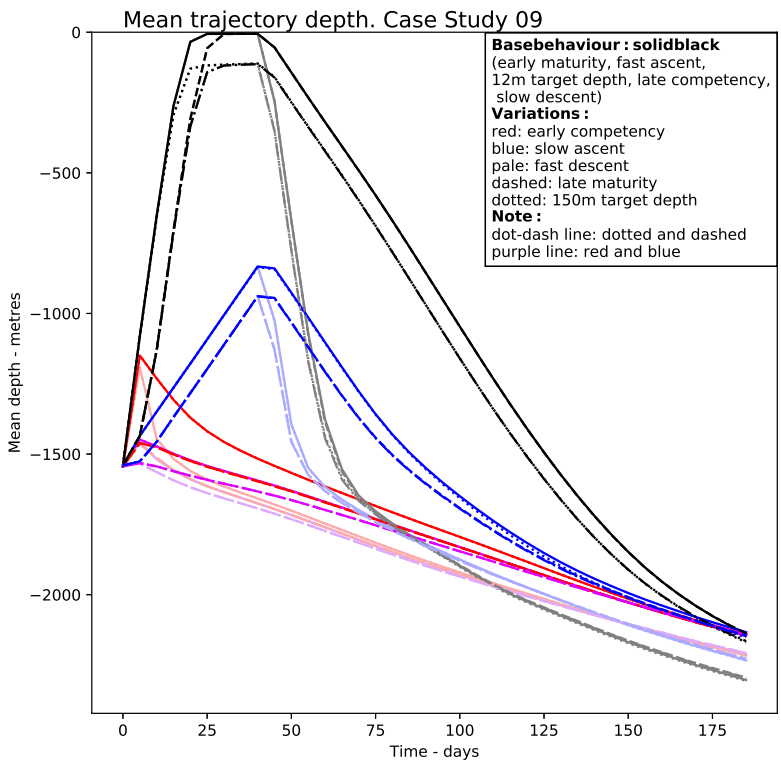

Figure 24: As Figure 16 but for Case Study 09, Reykjanes Ridge.

(a)

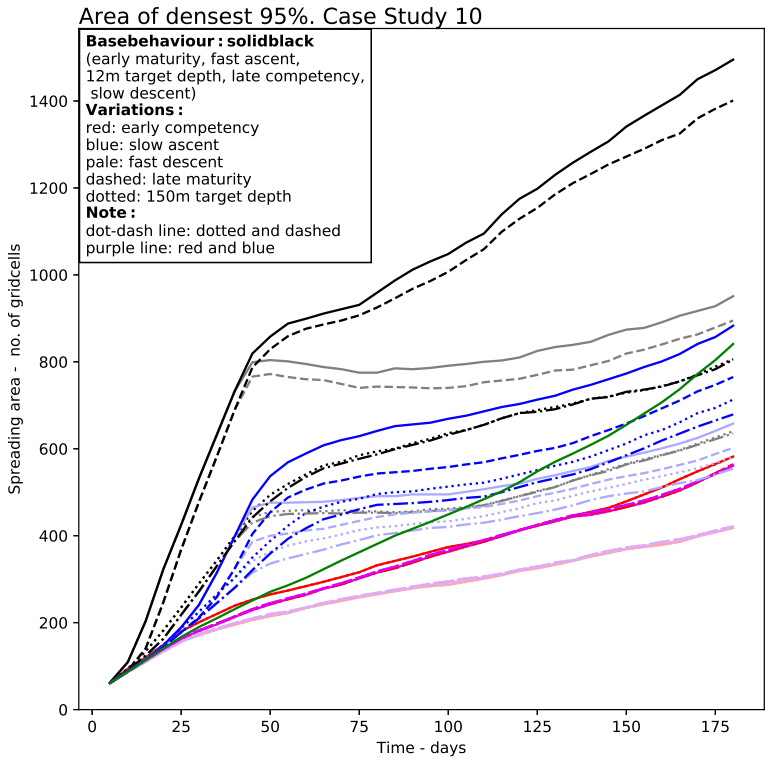

(b)

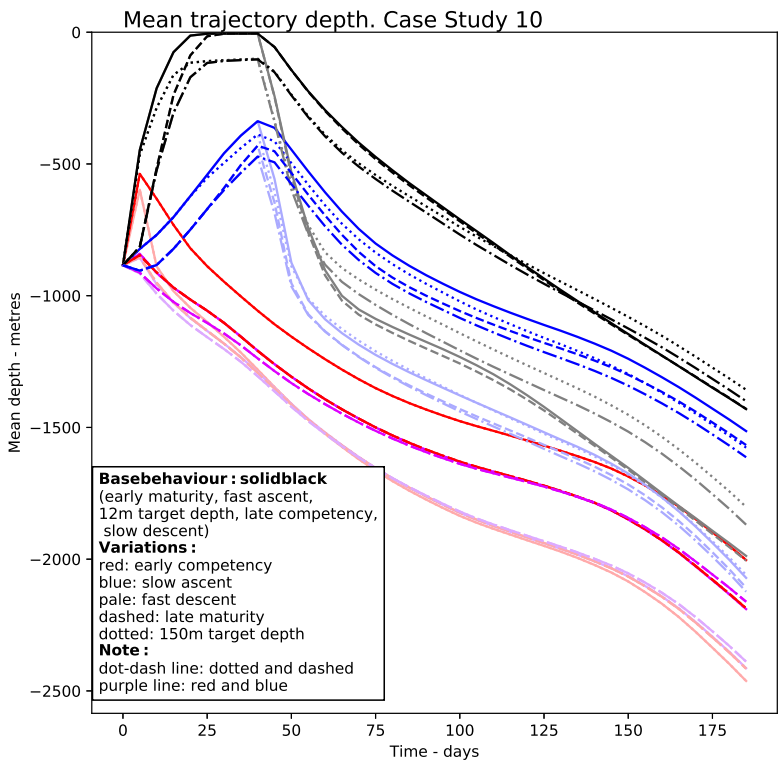

Figure 25: As Figure 16 but for Case Study 10, Davis Strait.

(a)

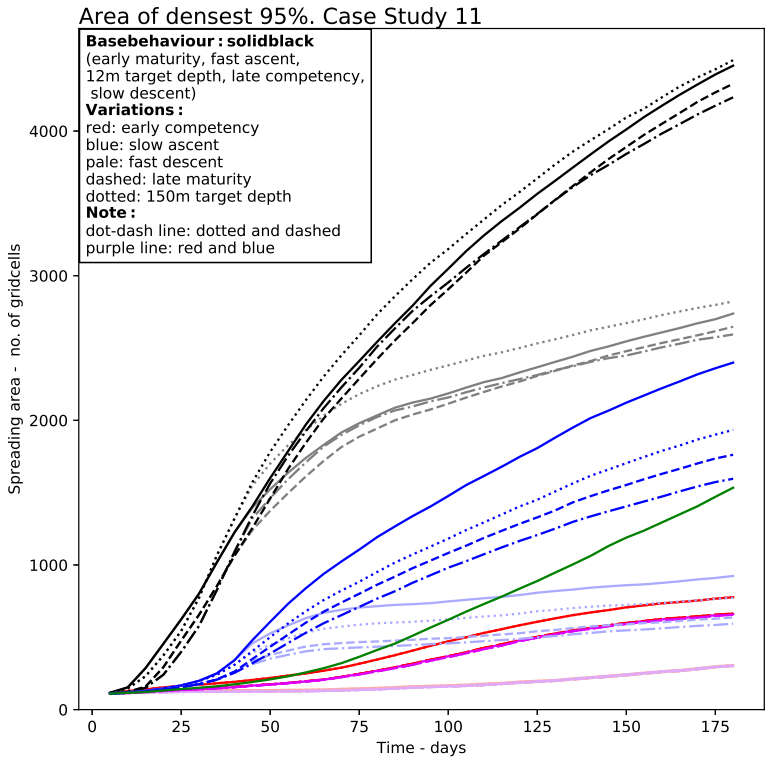

(b)

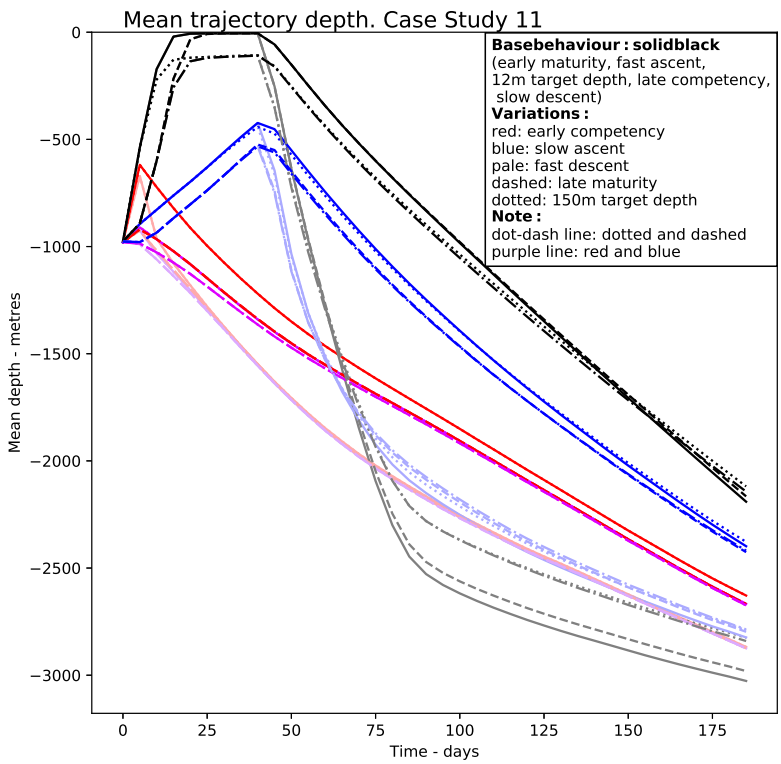

Figure 26: As Figure 16 but for Case Study 11, Flemish Cap

(a)

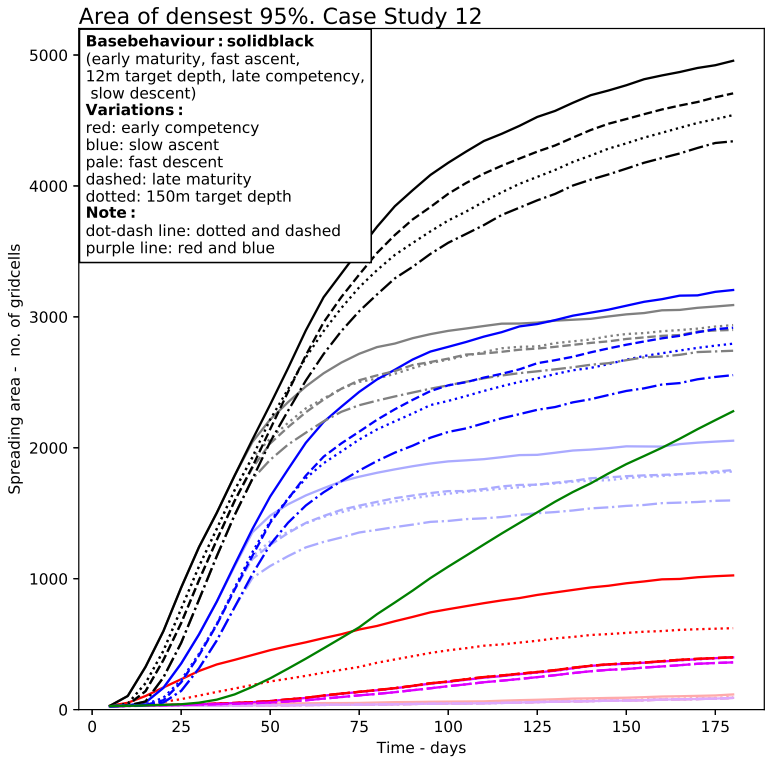

(b)

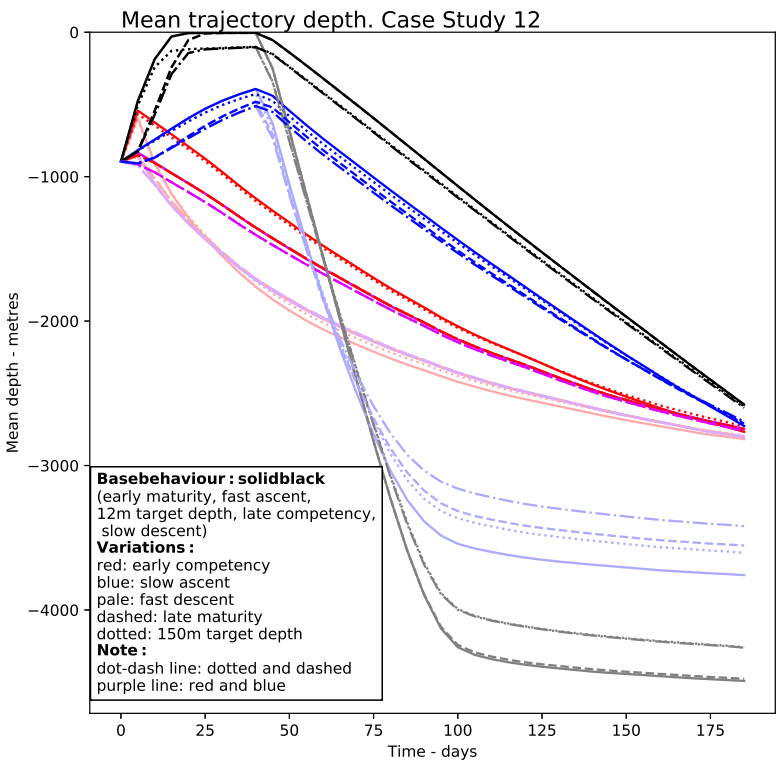

Figure 27: As Figure 16 but for Case Study 12, US Mid-Atlantic Canyons

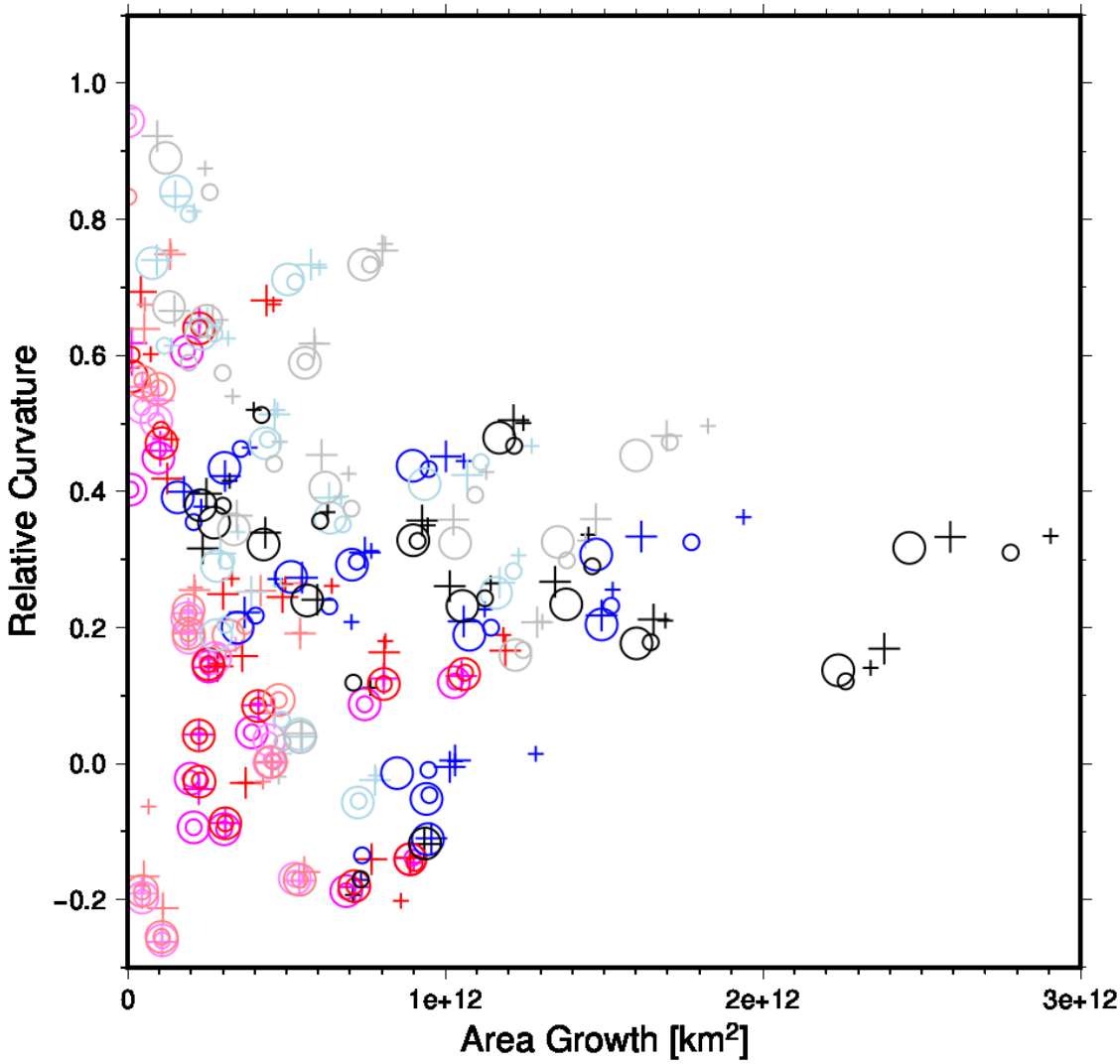

Figure 28: Area growth index versus relative curvature in the area grow index for each Case Study and each of the 32 combinations of larval behaviours. The indices are defined in Section 2. Colours correspond to the larval behaviour colours defined in Table 2. Since scatter plots cannot use line types, the different line types of Table 2 are replaced by changes in symbol type. Early (late) maturity is differentiated by plus (open circle) symbols while shallow (deep) target depth is indicated with smaller (bigger) symbols.

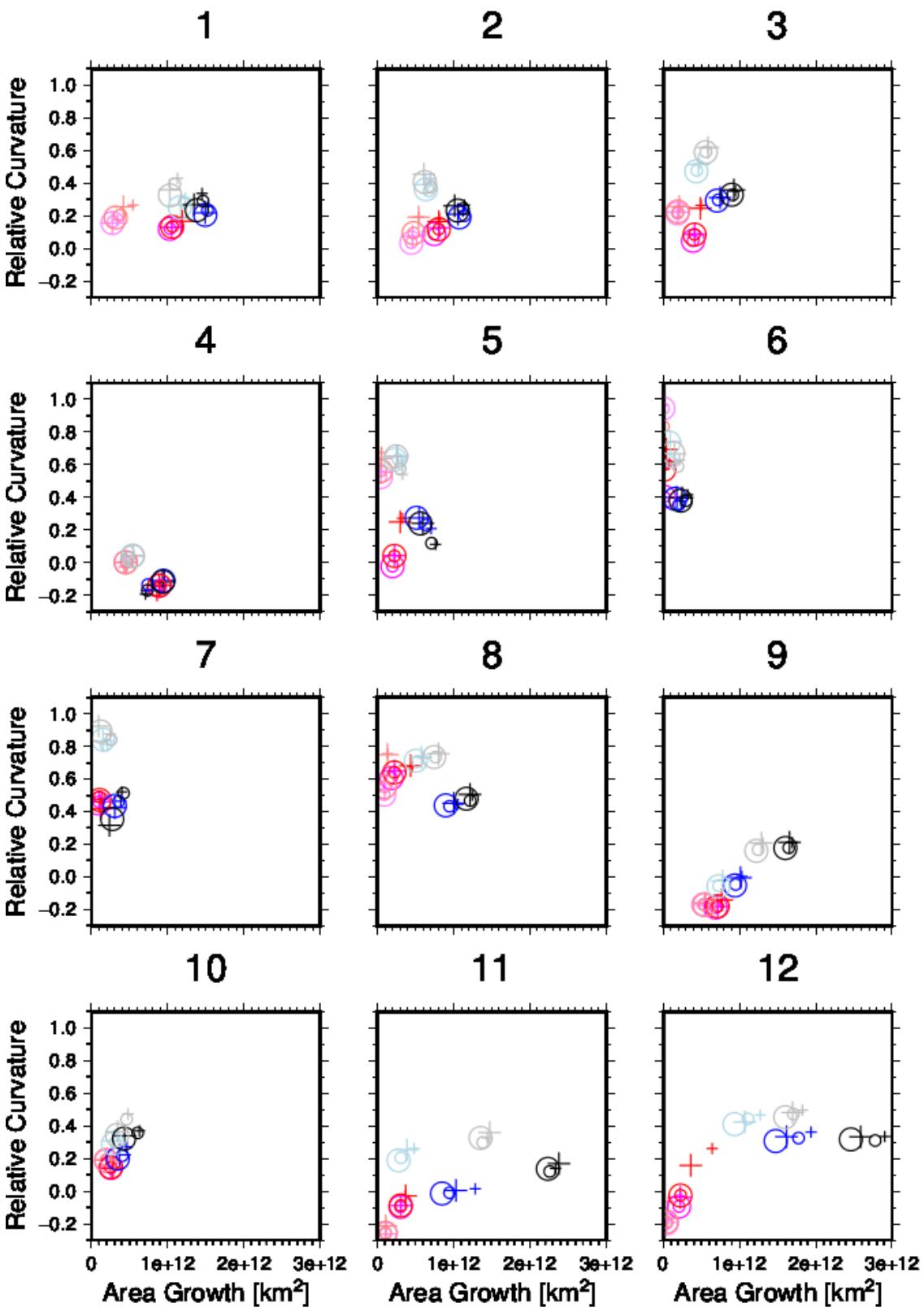

Figure 29: As in Figure 28 but with a separate panel for each Case Study. Case Studies are numbered above each figure.

Document Information

EU Project Nº	678760	**Acronym**	ATLAS
Full Title	A trans-Atlantic assessment and deep-water ecosystem-based spatial management plan for Europe		
Project website	www.eu-atlas.org		

Deliverable	**Nº**	D1.6	**Title**	Biologically realistic Lagrangian dispersal and connectivity
Work Package	**Nº**	WP1	**Title**	Ocean Dynamics Driving Ecosystem Response

Date of delivery	**Contractual**	31/12/2018	**Actual**	29/12/2018
Dissemination level	Public			

Authors (Partner)	**UEDIN**			
Responsible Authors	**Name**	Alan Fox	**Email**	Alan.Fox@ed.ac.uk

Version log			
Issue Date	**Revision Nº**	**Author**	**Change**